UNIVERSIDADE DE SÃO PAULO

INSTITUTO DE FÍSICA DE SÃO CARLOS

AMILSON ROGELSO FRITSCH

Thermodynamics of a Bose gas: Sound velocity from global variables and equivalence with other approaches

São Carlos

2016

AMILSON ROGELSO FRITSCH

Thermodynamics of a Bose gas: Sound velocity from global variables and equivalence with other approaches

Thesis presented to the Graduate Program in Physics at the Instituto de Física de São Carlos, Universidade de São Paulo to obtain the degree of Doctor of Science.

Concentration area: Basic Physics
Advisor:
Prof. Dr. Emanuel A. L. Henn

Corrected Version

(Original version available on the Program Unit)

São Carlos

2016

Cataloguing data reviewed by the Library and Information Service
of the IFSC, with information provided by the author

Fritsch, Amilson Rogelso
Thermodynamics of a Bose gas: Sound velocity from global variables and equivalence with other approaches / Amilson Rogelso Fritsch; advisor Emanuel Alves de Lima Henn - reviewed version -- São Carlos 2016.
106 p.

Thesis (Doctorate - Graduate Program in Basic Physics) -- Instituto de Física de São Carlos, Universidade de São Paulo - Brasil , 2016.

1. Global variables. 2. Sound velocity. I. Henn, Emanuel Alves de Lima, advisor. II. Title.

With love, to

my family and Joyciane my love

Acknowledgements

Without question, this is one of the hardest part of the thesis, and where we can commit a mistake forgetting people that helped in this thesis. Therefore, if this occurs, my sincere apologies.

I would like to thank my family for their love. For believe me and wish me all the best, for the education and the support. Live far from the family is not easy, but the talks and a few visits help us, and also motivate me to return.

A lovely person who helps me in everything, also makes it more easy, and is always on my side. This is my wife. Thank you Joyciane, for help me in everything, for your love, dedication, your patience, mainly in this days of writing the thesis and with the classes, our time together becomes short, but you supported me always. Also for her family, my second family, for their love, confidence, and to consider me as a son.

My supervisor Emanuel, for the time dedicated to this thesis. For the patience in reading and correcting this thesis many times, and for teaching me during this period. We know that the orientation is not an easy task but he accepted it and did everything possible to improve the quality of this work.

To Vanderlei, who is not my supervisor but is as if he were. For the good discussions about physics, for good classes of deep learning. For accepted me in his group and for his friendship. I don't know how he is able to make 1000 things at the same time, and still he has time to think about science and to plan new measurements.

The experiment team: Pedro and Franklin ("*los caras* de égua") for all days sharing the experiment, making jokes, discussing about useless things. But especially for the friendship, that is not just during the time at the experiment. Pedro, with his extensive experience at this experiment, teaching a lot about the problems (that are not just a few) and the solutions. For others actual and past members, Abasalt, Rodrigo, Gustavo, Arnol, for the productive discussions, for solving the experiment problems, and also for all the

time dedicated to the experiment. Giacomo, that when present motivate me a lot for his excitement in discussing physics, and also for his great knowledge and experience.

For all lab friends and collaborators: Edwin, Emmanuel (Emma), Patrícia, Kilvia, Freddy, Jorge, Rafael, Anne, Andrés, Jair, Rodrigo, Prof. Daniel, Prof. Sérgio, Prof. André, Prof. Ricardo. For the collaboration in the experiment, exchanging and sharing equipment, knowledge and information.

For theoreticians, Andre, Ednilson, Marios, Monica, Alexsandr, for the great collaboration at the experiment, with numerical simulations, suggestions, and for the help in make some concepts more clear.

The LIEPO team, that gives support for the equipment, circuits and electronics, whose team I will not cite everybody since there are a lot of new people and I will surely forget most of them. But João, Denis, Leandro, Gilherme, André, were whom I had more friendship and productive talks.

For all professors that I had during my formation, for all transferred knowledge, and for his dedication.

All other members of the optics group and IFSC, post-graduation service, library, the secretaries, and the team of the mechanical workshop, the for the support with the bureaucracy, the projects, travels, shopping, and many other things.

And one more time, I apologize who I forget to cite. It will be not easy to remember a person only after the thesis deposit, but I will be grateful for everybody who helps me in this thesis.

USP and IFSC for participating and improving my formation.

CAPES, FAPESP and CNPq, for my scholarship and also the financial support for this project.

Abstract

FRITSCH, A. R. **Thermodynamics of a Bose gas: Sound velocity from global variables and equivalence with other approaches**. 2016. 103 p. Thesis (Doctorate in Science) - Instituto de Física de São Carlos, Universidade de São Paulo, São Carlos, 2016.

In this thesis we present some studies that were done in a trapped ^{87}Rb Bose-Einstein condensate using the thermodynamic global variables. We have measured the global sound velocity by studying the variation of the total number of trapped atoms as a function of temperature. This method allowed us to determine the contribution of thermal and BEC components at each temperature. In order to study the sound velocity in each component, we treated both fluids as they were completely independent and we found great similarity with a published work. In addition, we analyze theoretically the validity of the global variables by comparing this approach with other methods. The specific heat for an ideal gas was evaluated using the global variables and by using the usual statistical approach found in textbooks. After finding the same result for both methods, we used the simplicity to implement the interaction in the global approach, to study the variation in the specific heat when the interactions are taken into account. The last comparison was done between global variables and the local density approximation. We have obtained that, for the isothermal compressibility and a equation of state, both methods provide equivalent results.

Keywords: Bose-Einstein condensation. Global variables. Sound velocity.

Resumo

FRITSCH, A. R. **Termodinâmica de um gás de Bose: Velocidade do som a partir de variáveis globais e equivalência com outros métodos**. 2016. 103 p. Tese (Doutorado em ciências) - Instituto de Física de São Carlos, Universidade de São Paulo, São Carlos, 2016.

Nesta tese descrevemos estudos que foram feitos em um Condensado de Bose-Einstein de ^{87}Rb usando variáveis termodinâmicas globais. A velocidade do som foi medida através de variações do número de átomos aprisionados em função da temperatura. Com este método fomos capazes de determinar qual a contribuição da componente térmica e do condensado em cada temperatura. Com o objetivo de estudar a velocidade do som em cada componente, analisamos ambas componentes como se elas fossem totalmente independentes, e encontramos grande similaridade com outro trabalho publicado. Adicionalmente, um estudo teórico foi feito para analisar a validade das variáveis globais comparando com outros métodos. O calor específico para um gás ideal foi calculado usando as variáveis globais e também usando o tratamento estatístico convencional encontrado em livros-texto. Depois de encontrar os mesmos resultados com os dois métodos, usamos a facilidade que temos em considerar as interações entre os átomos usando as variáveis globais, e estudamos a variação no calor específico quando estas interações são consideradas. Em um último estudo, comparamos as variáveis globais com o método de aproximação da densidade local. Para a compressibilidade isotérmica e para uma equação de estado obtemos resultados equivalentes com os dois métodos.

Palavras-chaves: Condensação de Bose-Einstein. Variáveis globais. Velocidade do som.

List of Figures

List of abbreviations and acronyms

BEC	Bose-Einstein condensation/condensate.
GPE	Gross-Pitaevskii equation.
TFA	Thomas-Fermi approximation.
GV	Global Variables.
MOT	Magneto-Optical Trap.
MOT1	Magneto-Optical Trap produced in the first chamber.
MOT2	Magneto-Optical Trap produced in the second chamber.
QUIC	Quadrupole-Ioffe configuration.
RF	Radio frequency.
PSD	Phase-space density.
TOF	Time-of-flight.
CCD	Charge-coupled device.
OD	Optical density.
LDA	Local density approximation.
EoS	Equation of state.

Contents

1 Introduction

Bose-Einstein condensation was predicted by Albert Einstein in 1925 after a generalization of the Bose studies for the black-body radiation. (1–2) The Bose-Einstein condensation, as it is known, occurs when at very low temperatures a gas of bosons macroscopically occupy the lowest-energy state of the system, the fundamental state. (3)

Condensation can be considered as a macroscopic and coherent occupation of the same state, where every atom is equal to all other, and all them behave equally. The phenomenon can be visualized if we consider the superposition of the wave function of the atoms. When atoms are cooled until the temperature where the de Broglie wavelength becomes at the order of the separation between atoms, the wavefunctions will overlap and will produce a condensate.

Since the prediction until the first evidence of the condensation it has passed many years. In 1938 London (4) suggested that the superfluidity observed in the liquid helium (5–6) could be associated to the Bose-Einstein condensation.

In dilute gases, Bose-Einstein condensation occurs at very low temperatures. This made the condensation a very difficult task, and it took almost six decades to be achieved. As it has always been, the hydrogen is the easiest element to be theoretically described, then is natural to think that it would be a good choice to obtain the condensation. Motivated by theoretical studies (7–8), in 1976 a group led by Greytak and Kleppner at MIT (9) started the attempt to condensate hydrogen, but it showed to be a formidable task. Many techniques to cool hydrogen were developed (10–13), but at the same time many groups started to work in cooling and trapping alkali atoms.

For alkali atoms, many techniques of coolling and trapping (11, 14–20) where developed, and along years lower temperatures and higher densities were achieved. When the evaporative cooling technique developed for hydrogen received an inportant improvement (21), it seemed to be the last step to condensation.

Finally, condensation was obtained in 1995 by the group of E. A. Cornell and C. E. Wieman in ^{87}Rb (22), in ^{23}Na by the group of W. Ketterle (23), and in ^{7}Li by the group led by R. G. Hulet. (24)

In our group, condensation was obtained in 2004 in ^{23}Na (25), but some experimental limitations have motivated the construction of a new experiment, for Rubidium atoms. (26) In the beginning, the group tested a new method to excite the condensate, using oscillatory magnetic field, and it culminated with the generation of vortices and tangle of vortices (27–31) which allowed to study quantum turbulence. (32–33) The latter has been one of the main focus of the group.

Another area that the group has great interest is thermodynamics, but due to difficulties in defining valid thermodynamic variables for trapped gases, there are not many experimental works exploring this field. In most of cases, BEC is achieved in an harmonic trapping potential, what makes the density of the sample not be uniform. This non-uniform density implies that the pressure and other variables are dependent on the position.

To overcome the inconvenient of a non-uniform density, it can be applied the local density approximation (LDA) (34), that allows to obtain most properties of the gas, such as the specific heat and the compressibility. (35) In this approximation, the sample is divided in small cells where the density is considered to be uniform, and it can only be used when the density inside each cell varies smoothly. For each cell is defined a set of independent thermodynamic variables, and it is clear that in this approximation we do not define parameters for the trapped gas as a whole.

This approximation is valid when the density of the gas varies smoothly. If a vortex is present in a cloud, the density varies abruptly in the border of the core, and we need to choose a cell much smaller than the vortex to avoid that a single cell contains the frontier (avoiding abrupt variations). From the theoretical point of view this is not a problem, because always is possible to choose the size of the cell to be very small. However, the experimental limitation is that the size of a BEC is of the order of microns, and the cell would need to be much smaller. In this case, would be very hard to determine the number

of atoms and other quantities for each cell.

In the search for a global thermodynamic description of trapped gases, the group and collaborators have developed the thermodynamic global variables. (36–37) In this approach, it is assumed that the trapped gas can be described by global parameters associated with the atoms as well as the trapping potential.

These global variables where proposed in 2005 (36–37) and since them they were successfully applied to a trapped Bose gas. (36, 38–42)

With the objective of validate and consolidate the global variables, we developed this thesis focusing in thermodynamics, where we used them to evaluate the sound velocity in a Bose gas and also we compared this approach with other methods.

In what follows, we describe how this thesis is organized and

1.1 This thesis

This thesis was developed in a experiment where we focus in two main research areas: Quantum turbulence and thermodynamic of trapped gases. For studying quantum turbulence, the main technique is to perturb the condensate by using an oscillatory magnetic field. In 2009 (32) this method was applied and the first evidence of quantum turbulence was observed.

During this project, we have worked in understanding the effects of this perturbations, mainly in the transition from a non perturbed state to an state were evidences of turbulence is found. The main studies were published in references (33, 43–44) and other are submitted or in preparation. Also, in search for new methods to produce turbulence, we have successfully implemented the technique of topological phase imprinting (45–46) to produce multicharged vortices. The decay of this multicharged vortex into unit charge vortices is not completely understood and is constantly under investigation.

Thermodynamic is the other research area of interest. To understand more about thermodynamic in trapped gases, the group have used the global thermodynamic variables (36–37) that have been developed to study the global properties of a trapped sample. In the BEC1 experiment, where this thesis has been developed, we cannot change the trapping frequencies, and it limits the studies that can be done in thermodynamic. However, another experiment was built a few years ago with a different technique to trap atoms, using a combination of optical and magnetic trap, instead a pure magnetic trap. In that system, the trapping volume can be easily changed, allowing a broader study. I could work for a short time in that experiment, where we have measured the isothermal compressibility of a Bose gas. (42)

This thesis does not contain the studies performed with vortices and turbulence, and to see our studies about this topic we recommend the reader to reference (47) which is a thesis that had been developed at almost the same time, and whose focus is on that other area.

In this thesis, we present more evidences that the global thermodynamic variables can be used to study thermodynamic properties of the condensate, mainly in cases where the potential is not uniform. We compare this variables with the local density approximation and also we present an alternative measurement for the sound velocity.

We start Chapter 2 revisiting the theoretical description of a Bose gas trapped in a harmonic potential. The concepts involved in this chapter will give us theoretical support for the others. Many textbooks make a complete description for an ideal Bose gas in a *box* potential, but since our trap is *harmonic*, in Section 2.1 we treat only this specific trapping geometry. In Section 2.2, we review the weakly interacting Bose gas, where we show that when the kinetic energy of the atoms is ignored, the atomic density exhibits a parabolic shape, that is proportional to the inverse of the trapping potential.

In Chapter 3, we make a description of the global variables. We start defining the global parameters for an ideal gas and then we treat a more realistic system where the interactions are considered. We finish the chapter obtaining the pressure parameter for our specific harmonic potential.

Chapter 4 is used to describe our experimental system. We have separated it in sections whose sequence is the same of the experimental process used to obtain condensation. We do not make a very detailed description for every processes, since most of them are common for many experiments with BEC, and also this experiment is exhaustively detailed in previous thesis of our group. (48–49)

After the theory and the experimental description, we start detailing the studies which compose this thesis. In order to test the validity of the global variables, we make a theoretical study to compare it with other approaches. We start Chapter 5 evaluating the specific heat for an ideal gas using the global variables and also using the standard statistical treatment, and we show that they provide the same result. Since we can easily implement the interaction in the global approach, we used it to study the effect of the interaction in the specific heat. In Section 5.3 we evaluated the compressibility and an equation of state using the global variables and also the local density approximation. Using these two approaches, we can observe the characteristic behavior of the compressibility at the transition. For the equation of state, the compressibility as a function of the pressure was evaluated in both methods and we found equivalent results.

In Chapter 6, we describe our alternatively measurement for the sound velocity in a Bose trapped gas using global variables instead of make a density perturbation in the BEC. The background theory for the sound velocity is summarized in Section 6.1 and after this we present our method to obtain the sound velocity. We finish this chapter by presenting the results for this study, where we could evaluate the contribution of the individual components, normal and BEC, for the sound velocity. We could also separate the two fluids to analyze them as if they were independent. In both analysis we found good agreement with the theory and also with measurements.

Finally, in Chapter 7, we conclude this thesis summarizing the results that where described in previous chapters, and after this we list possibles studies and improvements that will be done in our experimental system.

2 Statistical description for a trapped Bose-gas in harmonic potentials

Bose-Einstein condensation is well described in many textbooks of statistical mechanics. We start with an overview of the statistical description of the non interacting Bose gas confined in a harmonic external potential based on references (50–52), and in references (53–54) for the case where the interaction between particles is taken into account. At the beginning of the chapter we focus on finding the grand canonical potential and the critical temperature, which allows us to easily find other important variables, and will also give support to define the global variables which are explained in Chapter 3.

2.1 The ideal Bose gas trapped in a harmonic potential

In order to statistically describe a Bose gas in a harmonic potential, it is convenient to work in the context of the grand canonical ensemble, where the total number of particles in the system is not fixed. In this ensemble, we can obtain much information about the thermodynamic properties of the gas by just taking simple derivatives of the grand canonical potential Ω. Among these thermodynamic properties, we can cite entropy, pressure, and number of atoms of the system, given respectively by (51)

$$S(\mu, T, V) = -\left[\frac{\partial \Omega}{\partial T}\right]_{V,\mu}, \tag{2.1}$$

$$p(\mu, T, V) = -\left[\frac{\partial \Omega}{\partial V}\right]_{T,\mu}, \tag{2.2}$$

$$N(\mu, T, V) = -\left[\frac{\partial \Omega}{\partial \mu}\right]_{T,V}, \tag{2.3}$$

where T, V and μ are the temperature, volume and chemical potential of the system.

In order to derive the grand canonical potential, we start by writing the Hamiltonian for this system

$$H_N = \sum_j \left(\frac{P_j^2}{2m} + U(r_j)\right), \tag{2.4}$$

where P_j is the momentum for each particle with mass m, and $U(r_j)$ is the external potential. Here if the interaction between particles is taken into account, an additional term must be considered.

Our external potential is a harmonic oscillator

$$U(r_j) = \sum_j \frac{1}{2} m \left(\omega_x^2 x_j^2 + \omega_y^2 y_j^2 + \omega_z^2 z_j^2\right), \tag{2.5}$$

where m is the mass of the particles and $\omega_x, \omega_y, \omega_z$ are the frequencies of the oscillator. Writing the external potential, the Hamiltonian takes the form

$$H = \sum_j \left[\frac{P_j^2}{2m} + \frac{1}{2} m \left(\omega_x^2 x_j^2 + \omega_y^2 y_j^2 + \omega_z^2 z_j^{2,}\right)\right] \tag{2.6}$$

which can be written in a more suitable form in terms of the occupation number

$$H_N = \sum_j \hbar \left[\omega_x \left(n_x^j + \frac{1}{2}\right) + \omega_y \left(n_y^j + \frac{1}{2}\right) + \omega_z \left(n_z^j + \frac{1}{2}\right)\right]. \tag{2.7}$$

Now we will write the grand canonical potential function $\mathcal{Z}$, given by (50)

$$\mathcal{Z} = \sum_{N=0}^{\infty} e^{\beta \mu N} \sum_{n_j} e^{-\beta \epsilon_j n_j}, \tag{2.8}$$

where N is the total number of particles in all possible states, μ is the chemical potential and $\beta = 1/k_B T$ with k_B the Boltzmann constant and T the temperature. The number of particles in the state j, which has energy ϵ_j, is $\{n_j\}$, and the total energy of this state is $E\{n_j\} = \sum_j \epsilon_j n_j$. For the Hamiltonian of Equation 2.7, $\epsilon_j n_j = \hbar(\omega_x n_x^j + \omega_y n_y^j + \omega_z n_z^j) + E_0$

where $E_0 = \frac{\hbar}{2}(\omega_x + \omega_y + \omega_z)$ is the ground-state energy of the system. Writing the total number of particles as $N = \sum_j n_j$ we have

$$\mathcal{Z} = \sum_{N=0}^{\infty} \exp\left[\beta\mu n_1 + \beta\mu n_2 + \ldots\right] \sum_{n_j} \exp\left[-\beta\epsilon_1 n_1 - \beta\epsilon_2 n_2 - \ldots\right] \tag{2.9}$$

$$= \sum_{N=0}^{\infty} \sum_{n_j} \exp\left[-\beta(\epsilon_1 - \mu)n_1 - \beta(\epsilon_2 - \mu)n_2 - \ldots\right]. \tag{2.10}$$

The sum in n_j, which is done for each occupation number n, is also performed for the total number of particles, $N = n_1 + n_2 + \ldots$, what allow us to write

$$\mathcal{Z} = \sum_{n_1} \exp\left[-\beta(\epsilon_1 - \mu)n_1\right] \sum_{n_2} \exp\left[-\beta(\epsilon_2 - \mu)n_2\right] \ldots \tag{2.11}$$

$$= \prod_{j=0}^{\infty} \sum_{n=0}^{\infty} \exp\left[-\beta(\epsilon_j - \mu)n\right]. \tag{2.12}$$

The sum in the last equation is a geometric series of the form

$$\sum_{n=0}^{\infty} \exp\left[-\beta(\epsilon_j - \mu)n_n\right] = \frac{1}{1 - \exp\left[-\beta(\epsilon_j - \mu)\right]}, \tag{2.13}$$

which leads to write the grand partition function as

$$\mathcal{Z} = \prod_{j=0}^{\infty} \left\{ \frac{1}{1 - \exp\left[-\beta(\epsilon_j - \mu)\right]} \right\}. \tag{2.14}$$

Since from Equation 2.8 we have written the energy ϵ_j of each state j in a general way, the last equation is general for any system, not restricted to an harmonic oscillator.

As discussed in the beginning of this chapter, we can easily obtain some useful relations by using the grand thermodynamic potential Ω, which is related to the grand partition function by (50)

$$\Omega(\mu, T, V) = -k_B T \ln \mathcal{Z}. \tag{2.15}$$

Using Eq. 2.14, we find the grand thermodynamic potential for an ideal gas, given by

$$\Omega(\mu, T, V) = -k_B T \sum_{j=0}^{\infty} \ln\left\{1 - \exp\left[-\beta(\epsilon_j - \mu)\right]\right\}, \tag{2.16}$$

and by Equation 2.3 we see that after a simple derivation of Equation 2.16 with respect to the chemical potential, we get the total number of atoms

$$\bar{N} = \sum_{j=0}^{\infty} \bar{n_j}, \tag{2.17}$$

with

$$\bar{n_j} = \frac{1}{\exp\left[\beta(\epsilon_j - \mu)\right] - 1}. \tag{2.18}$$

The last equation is the Bose distribution, where $\bar{n_j}$ gives the mean number of Bosons in each state j. From this equation we can conclude that $\exp\left[\beta(\epsilon_j - \mu)\right] > 1$ always holds, or $\epsilon_j > \mu$, and since the chemical potential must be smaller than the energy of the lowest level ϵ_0 ($\epsilon_0 = 0$), μ must be always negative. If we consider $\mu > 0$ and $\epsilon_0 = 0$, then n_0 would be negative, which is not possible.

We can also observe that when the number of particles is fixed, a decrease in temperature leads to an increase in the chemical potential and it tends to zero, resulting in the Bose-Einstein condensation, which means that adding more particles to the system will cost no energy.

When the spacing between two energy levels becomes small, we can replace sums by integrals making $\sum_\epsilon = \int g(\epsilon)d\epsilon$, where $g(\epsilon)$ is the density of space . Using the standard procedures described in textbooks (51,54) we obtain the density of states for an harmonic oscillator by evaluating the number of states $G(\epsilon)$ enclosed in an energy surface of radius $\epsilon = \epsilon_x + \epsilon_y + \epsilon_z$. This is done by

$$G(\epsilon) = \frac{1}{\hbar^3(\omega_x\omega_y\omega_z)} \int_0^\epsilon d\epsilon_x \int_0^{\epsilon-\epsilon_x} d\epsilon_y \int_0^{\epsilon-\epsilon_x-\epsilon_y} d\epsilon_z = \frac{\epsilon^3}{6\hbar^3\bar{\omega}^3}, \tag{2.19}$$

where $\bar{\omega} = (\omega_x\omega_y\omega_z)^{1/3}$ is the geometric mean of the trap frequencies. The density of states is

$$g(\epsilon) = \frac{dG(\epsilon)}{d\epsilon}, \tag{2.20}$$

then

$$g(\epsilon) = \frac{1}{2}\frac{\epsilon^2}{(\hbar\bar{\omega})^3}. \tag{2.21}$$

The density of states can be generalized for a d-dimensional harmonic oscillator and results in (54)

$$g(\epsilon) = \frac{\epsilon^{d-1}}{(d-1)!\prod_{i=1}^{d}\hbar\omega_i}. \tag{2.22}$$

Here we need to pay attention that in Equations 2.16 and 2.17 there can be a state with $\epsilon = 0$, but if we consider just the replacement from sum to integrals using

Equation 2.21 this state disappear because $g(0) = 0$, and it will lead to a mistake. To make a correct replacement we need to take into account the term with $\epsilon = 0$, what leads to an additional term in both equations after the replacement. It will lead Equation 2.17 to be written as

$$N = \frac{1}{2(\hbar\bar{\omega})^3}\int_0^\infty \frac{\epsilon^2}{\exp\left[\beta(\epsilon-\mu)\right]-1}d\epsilon + N_0, \tag{2.23}$$

where $N_0 = z/(1-z)$ is the number of atoms in the ground state ($\epsilon = 0$) and $z = \exp\beta\mu$ is the fugacity.

For the grand canonical potential, Equation 2.16, we have

$$\Omega(\mu,T,V) = \frac{-1}{2\beta(\hbar\bar{\omega})^3}\int_0^\infty \epsilon^2 \ln\left\{1-\exp\left[-\beta(\epsilon-\mu)\right]\right\}d\epsilon + \frac{1}{\beta}\ln(1-z), \tag{2.24}$$

which becomes

$$\Omega(\mu,T,V) = \frac{1}{6(\hbar\bar{\omega})^3}\int_0^\infty \frac{\epsilon^3}{z^{-1}\exp(\beta\epsilon)-1}d\epsilon + \frac{1}{\beta}\ln(1-z). \tag{2.25}$$

If we write $x = \beta\epsilon$ in Equations 2.23 and 2.25, we see that both integrals can be expressed in the form

$$g_n(z) = \frac{1}{\Gamma(n)}\int_0^\infty \frac{x^{n-1}}{z^{-1}\exp(x)-1}dx = \sum_1^\infty \frac{z^k}{k^n}, \tag{2.26}$$

which is known as the Bose function (51) and $\Gamma(n)$ is the Gamma function. Using the last expression we can write the number of atoms and the grand canonical potential as

$$N = \frac{1}{2(\beta\hbar\bar{\omega})^3}g_3(z)\Gamma(3) + N_0, \tag{2.27}$$

$$\Omega = \frac{1}{6\beta^4(\hbar\bar{\omega})^3}g_4(z)\Gamma(4) - \frac{1}{\beta}\ln(1-z). \tag{2.28}$$

For $z = 1$, it means $\mu = 0$, the Bose function is related to the Riemann's Zeta function $\zeta(n)$, by

$$g_n(1) = \sum_{k=1}^\infty \frac{1}{k^n} = \zeta(n) \qquad n > 1, \tag{2.29}$$

which is very important in finding the maximum number of particles in the excited state*. We see in Equation 2.27 that the total number of particles is expressed as the sum of the

* Here the limit when $z = 1$ need to be analyzed with care. In principle, N_0 in Equation 2.23 and the grand canonical potential in Equation 2.28 are divergent, and both can not be determined in this condition. However, both are well determined when the thermodynamic limit is analysed. In this limit, the last therm in Equation 2.28 always is smaller than the first one, and can be neglected. We recommend the Chapter 13 of reference (51) for more details.

particles in the fundamental state (N_0 with $\epsilon = 0$) and the particles in the excited states N_e, the first term. As discussed, the chemical potential must be always negative and it establishes that 1 is the maximum value for z. Now, using Equation 2.29 we find that

$$N_e^{max} = N - N_0 = \frac{1}{2(\beta\hbar\bar{\omega})^3}\zeta(3)\Gamma(3) \tag{2.30}$$

is the maximum number of particles in the excited states.

If we fix the volume and the temperature of the gas and we add particles, the population of the excited states cannot increase beyond its maximum value, and the ground state becomes macroscopically populated, which leads to the Bose-Einstein condensation. Thus, Equation 2.30 defines the critical temperature where it occurs, and if we suppose that at this temperature $N_0 \ll N$ we obtain

$$T_c = \frac{\hbar\bar{\omega}}{k_B}\left(\frac{N}{\zeta(3)}\right)^{1/3} \approx 0.94\frac{\hbar\bar{\omega}}{k_B}N^{1/3}. \tag{2.31}$$

Using this temperature, we can find the population of the ground state as a function of the temperature. Dividing 2.27 by N and using the critical temperature, we find

$$\frac{N_0}{N} = 1 - \left(\frac{T}{T_c}\right)^3, \tag{2.32}$$

that shows the dependence of the condensed fraction with the temperature.

2.2 Weakly interacting Bose gas

In the previous section we just considered an ideal Bose gas in a harmonic potential. However, in experiments with Bose-Einstein condensates, the density is relatively high and a complete description of the condensed properties must include interactions. When interactions are taken into account we can describe the condensate, at zero temperature [†] and in the regime of weak interaction, using the Gross-Pitaevskii equation (GPE), which

[†] At finite temperature large condensed fraction is necessary.

was formulated independently by E. Gross (55) and L. Pitaevskii (56) and has proved excellent to describe these systems. A more detailed discussion can be found in references. (53, 57–58)

2.2.1 The Gross-Pitaevskii equation

We can describe a system of N interacting bosons by using the Hamiltonian written in second quantization as (53)

$$\hat{H} = \int d^3\mathbf{r}\hat{\Psi}^\dagger(\mathbf{r},t)\left[-\frac{\hbar^2}{2m}\nabla^2 + U_{\text{ext}}(\mathbf{r})\right]\hat{\Psi}(\mathbf{r},t) \tag{2.33}$$

$$+\frac{1}{2}\int d^3\mathbf{r}\int d^3\mathbf{r}'\hat{\Psi}^\dagger(\mathbf{r},t)\hat{\Psi}^\dagger(\mathbf{r}',t)V(\mathbf{r}-\mathbf{r}')\hat{\Psi}(\mathbf{r}',t)\hat{\Psi}(\mathbf{r},t), \tag{2.34}$$

where $\hat{\Psi}^\dagger(\mathbf{r},t)$ and $\hat{\Psi}(\mathbf{r},t)$ represent the creation and annihilation of a boson at the position $\mathbf{r}$, U_{ext} is the external potential and $V(\mathbf{r}-\mathbf{r}')$ is the interaction potential.

The energy of the atoms in a dilute and cold gas is sufficiently low such that the collisions are characterized by the s-wave scattering length. These are considered elastic hard-sphere collisions between two atoms, and we can write the interaction potential as

$$V(\mathbf{r}-\mathbf{r}') = g\delta(\mathbf{r}'-\mathbf{r}) \tag{2.35}$$

where $g = 4\pi\hbar^2 a/m$, with a being the s-wave scattering length. Inserting the potential of Equation 2.35 into Equation 2.33 we obtain

$$\hat{H} = \int d^3\mathbf{r}\hat{\Psi}^\dagger(\mathbf{r},t)\left[-\frac{\hbar^2}{2m}\nabla^2 + U_{\text{ext}}(\mathbf{r})\right]\hat{\Psi}(\mathbf{r},t) + \frac{g}{2}\int d^3\mathbf{r}\hat{\Psi}^\dagger(\mathbf{r},t)\hat{\Psi}^\dagger(\mathbf{r},t)\hat{\Psi}(\mathbf{r},t)\hat{\Psi}(\mathbf{r},t), \tag{2.36}$$

where the dependence on $\mathbf{r}'$ was removed.

Now, in order to derive the system dynamics we are going to write the time evolution of $\hat{\psi}(\mathbf{r})$ using the Heisenberg picture with the Hamiltonian of equation 2.36. Knowing the Bose commutation relations

$$\left[\hat{\Psi}(\mathbf{r}',t), \hat{\Psi}^\dagger(\mathbf{r},t)\right] = \delta(\mathbf{r}-\mathbf{r}') \tag{2.37}$$

and

$$\left[\hat{\Psi}\left(\mathbf{r}',t\right),\hat{\Psi}\left(\mathbf{r},t\right)\right]=\left[\hat{\Psi}^{\dagger}\left(\mathbf{r}',t\right),\hat{\Psi}^{\dagger}\left(\mathbf{r},t\right)\right]=0 \tag{2.38}$$

we have

$$\begin{aligned}
i\hbar\frac{\partial\hat{\Psi}(\mathbf{r}',t)}{\partial t} &= \left[\hat{\Psi}\left(\mathbf{r}',t\right),\hat{H}\right], \\
&= \hat{\Psi}\left(\mathbf{r}',t\right)\hat{H}-\hat{H}\hat{\Psi}\left(\mathbf{r}',t\right), \\
&= \hat{\Psi}\left(\mathbf{r}',t\right)\hat{H}-\int d^{3}\mathbf{r}\hat{\Psi}^{\dagger}(\mathbf{r},t)\hat{H}_{0}\hat{\Psi}(\mathbf{r},t)\hat{\Psi}\left(\mathbf{r}',t\right) \\
&\qquad -\frac{g}{2}\int d^{3}\mathbf{r}\hat{\Psi}^{\dagger}(\mathbf{r},t)\hat{\Psi}^{\dagger}(\mathbf{r},t)\hat{\Psi}(\mathbf{r},t)\hat{\Psi}(\mathbf{r},t)\hat{\Psi}\left(\mathbf{r}',t\right), \\
&= \hat{\Psi}\left(\mathbf{r}',t\right)\hat{H}-\int d^{3}\mathbf{r}\left[\hat{\Psi}\left(\mathbf{r}',t\right)\hat{\Psi}^{\dagger}\left(\mathbf{r},t\right)-\delta(\mathbf{r}'-\mathbf{r})\right]\hat{H}_{0}\hat{\Psi}\left(\mathbf{r},t\right) \\
&\qquad -\frac{g}{2}\int d^{3}\mathbf{r}\left[\hat{\Psi}\left(\mathbf{r}',t\right)\hat{\Psi}^{\dagger}\left(\mathbf{r},t\right)-2\delta(\mathbf{r}'-\mathbf{r})\right]\hat{\Psi}^{\dagger}\left(\mathbf{r}\right)\hat{\Psi}\left(\mathbf{r},t\right)\hat{\Psi}\left(\mathbf{r},t\right), \\
&= \hat{\Psi}\left(\mathbf{r}',t\right)\hat{H}-\hat{\Psi}\left(\mathbf{r}',t\right)\hat{H}+\int d^{3}\mathbf{r}\hat{H}_{0}\hat{\Psi}\left(\mathbf{r},t\right)\delta(\mathbf{r}'-\mathbf{r}) \\
&\qquad +g\int d^{3}\mathbf{r}\hat{\Psi}^{\dagger}\left(\mathbf{r},t\right)\hat{\Psi}\left(\mathbf{r},t\right)\hat{\Psi}\left(\mathbf{r},t\right)\delta(\mathbf{r}'-\mathbf{r}),
\end{aligned}$$

where $\hat{H}_{0}=-\frac{\hbar^{2}}{2m}\nabla^{2}+U_{\text{ext}}(\mathbf{r})$. The last equation results in

$$i\hbar\frac{\partial\hat{\Psi}(\mathbf{r},t)}{\partial t}=\hat{H}_{0}(\mathbf{r})\hat{\Psi}(\mathbf{r},t)+g\hat{\Psi}^{\dagger}(\mathbf{r},t)\hat{\Psi}(\mathbf{r},t)\hat{\Psi}(\mathbf{r},t). \tag{2.39}$$

When the Bose-Einstein condensation occurs, a single state is macroscopically occupied, and we can make this by separating the Bose operator into two parts and treat the non condensed state as a perturbation. By splitting we have

$$\hat{\Psi}(\mathbf{r},t)=\psi(\mathbf{r},t)+\delta\hat{\Psi}(\mathbf{r},t) \tag{2.40}$$

where $\psi(\mathbf{r})=<\hat{\Psi}(\mathbf{r},t)>$ represent the condensed part and $\delta\hat{\Psi}(\mathbf{r},t)$ represent the atoms in other states. This is usually referred as the Bogoliubov approximation. Then, in the limit of zero temperature and weak interaction, we can consider that all particles are in the condensate, and we can ignore $\delta\hat{\Psi}(\mathbf{r},t)$. Making the substitution of 2.40 into 2.39 we find

$$i\hbar\frac{\partial\psi(\mathbf{r},t)}{\partial t}=\left[-\frac{\hbar^{2}}{2m}\nabla^{2}+U_{\text{ext}}(\mathbf{r})+g|\psi(\mathbf{r},t)|^{2}\right]\psi(\mathbf{r},t), \tag{2.41}$$

which is the time-dependent Gross-Pitaevskii equation. If we consider a non-interacting system, $g = 0$, the GPE becomes the Schrödinger equation.

For stationary solutions we can make the substitution $\psi(\mathbf{r}, t) = \phi(\mathbf{r})e^{-i\mu t/\hbar}$ in the GPE to have

$$\left[-\frac{\hbar^2}{2m}\nabla^2 + U_{\text{ext}}(\mathbf{r}) + g|\phi(\mathbf{r})|^2\right]\phi(\mathbf{r}) = \mu\phi(\mathbf{r}) \tag{2.42}$$

which is the time-independent GPE and μ is the chemical potential.

2.2.2 Thomas-Fermi approximation

For condensates with repulsive interactions and a large number of atoms, the interaction energy is much higher than the kinetic energy and the first term in the GPE can be neglected. This is the Thomas-Fermi approximation (TFA) (53–54), which leads to

$$\left[U_{\text{ext}}(\mathbf{r}) + g|\phi(\mathbf{r})|^2\right]\phi(\mathbf{r}) = \mu\phi(\mathbf{r}), \tag{2.43}$$

or

$$|\phi(\mathbf{r})|^2 = \frac{\mu - U_{\text{ext}}(\mathbf{r})}{g}. \tag{2.44}$$

This predicts that the density ($n(\mathbf{r}) = |\phi(\mathbf{r})|^2$) of an interacting gas takes the inverted shape of the potential where the gas is confined. Typically, Bose-Einstein condensation is achieved in harmonic potentials with the form $U_{\text{ext}}(\mathbf{r}) = \frac{1}{2}m\sum_j \omega_j^2 r_j^2$, $j = x, y, z$. For this potential we have

$$n(\mathbf{r}) = \frac{2\mu - m\sum_j \omega_j^2 r_j^2}{2g}. \tag{2.45}$$

We note that if $r \to \infty$ the density would become negative, which is not physical, thus we need to establish the limit when $n(\mathbf{r}) = 0$. This limit is then

$$\mu = \frac{1}{2}m\sum_j \omega_j^2 R_j^2, \tag{2.46}$$

where R_j are called the *Thomas-Fermi radii* and are the boundary for the existence of the condensed. With this condition, the correct way to write Equation 2.47 is

$$n(\mathbf{r}) = \left(\frac{2\mu - \sum_j \omega_j^2 r_j^2}{2g} \right) \Theta(R_j^2 - r_j^2), \tag{2.47}$$

where $\Theta(r)$ is the *Heaviside* function. The normalization condition will give the total number of atoms, $N = \int n(\mathbf{r}) d^3\mathbf{r}$, and using the condition of Equation 2.46 for determining where the Thomas-Fermi density is valid, we find the relation between the number of atoms and the chemical potential

$$N = \frac{8\pi}{15g} \left(\frac{2}{m\bar{\omega}^2} \right)^{3/2} \mu^{5/2}, \tag{2.48}$$

where $\bar{\omega}$ is the geometric mean of the oscillator frequencies. If we solve for μ we obtain

$$\mu = \left(\frac{15Na}{\bar{a}} \right)^{2/5} \frac{\hbar\bar{\omega}}{2}. \tag{2.49}$$

Here $\bar{a} = \sqrt{\frac{\hbar}{m\bar{\omega}}}$ is the characteristic length of the harmonic oscillator.

3 Global thermodynamic variables

Global thermodynamic variables (GV) have been defined as a new and alternative approach to describe thermodynamics in trapped gases in arbitrary potentials. The pressure depends on the density, and since in a harmonic trap the density of the trapped gas is not uniform, we can not write a single pressure which describe the whole system.

In order to study thermodynamics in this system, we can use the local-density approximation (LDA). In this approximation, the fluid is divided in many parts where the density is assumed to be constant, then is possible to attribute thermodynamic local variables for each position. Using this approximation, the thermodynamic variables still have dependence with the position and, for example, we can not assign a single pressure for the whole system. But, can we find equivalent parameters to describe all the system instead locally?

Global variables has a different meaning. In this approach, the purpose is to study the system as a whole by using appropriated global parameters. These variables were proposed in 2005 by Romero-Rochín and Bagnato (36–37) to study thermodynamic properties of trapped gases considering that the gas has only a global pressure and a global volume. This new approach was initially proposed for harmonic potentials but it can be generalized to arbitrary external potentials. (59) A detailed description for the global variables can be found in references (36–37), and in (40–42) measurements can be found. In this chapter we will introduce these variables, and in Chapter 6 we apply them to evaluate the first sound.

In Chapter 5 we will compare the validity of these two treatments for same properties of the gas, such as the specific heat, the compressibility, and the equation of state.

3.1 Volume and Pressure parameters

In Chapter 2 we have reviewed the statistical treatment for a non-interacting Bose gas in a harmonic trap potential. Although these systems are excellent to test and explore new concepts, the study of thermodynamics are not always appropriate. We need to observe that since the density of a cloud in harmonic traps is not uniform, the pressure, and many other thermodynamics variables, have different local values for the same cloud.

Bose-Einstein condensation occurs at a macroscopic level, thus is can be more appropriate to study thermodynamics by means of parameters that can be associated with the macroscopic system.

In the search for a global description of thermodynamics in trapped gases that new variables were proposed. The idea is that the gas with N atoms at a temperature T, can be described by a global pressure and a global volume parameters, and they are sufficient to obtain the equation of state for the gas.

We start by using fundamental thermodynamic relations and the grand canonical potential definition

$$U = TS - PV + \mu N \tag{3.1}$$

$$\Omega = U - TS - \mu N \tag{3.2}$$

to show that the grand canonical potential is related with the pressure and the volume by

$$\Omega = -PV. \tag{3.3}$$

We see from the last equation, that the grand thermodynamic potential is the product of an extensive (V) and a intensive thermodynamic variable (P). For harmonic traps, as it can be checked by Equation 2.28 in the thermodynamic limit

$$\Omega = \frac{1}{6\beta^4(\hbar\bar{\omega})^3} g_4(z)\Gamma(4),$$

the grand canonical potential of a non-interacting gas is proportional to the frequencies of the trap, instead its volume.

Since many properties for this systems are obtained from derivation of the grand canonical potential, we conclude that the trapping frequency is a thermodynamic variable. (36) For a fixed number of atoms, any variation of the trapping frequencies will modify the temperature and the entropy of the atoms.

With this argument, we motivate the definition of a variable proportional to the trapping frequencies, given by

$$\mathcal{V} = \frac{1}{\omega_x \omega_y \omega_z} = \frac{1}{\bar{\omega}^3}, \tag{3.4}$$

that is called as *harmonic volume parameter* because it was originally defined for *harmonic* trap potentials. The quantity $\bar{\omega}$ is the geometric mean of the harmonic oscillator frequencies, and is often used to simplify the calculations. Obviously the volume parameter does not have units of the real spatial volume. Nevertheless, for a harmonic trap, small trapping frequencies imply in a higher physical volume of the cloud than for a trap with higher trapping frequencies, what gives for the volume parameter the same interpretation as the physical volume of a bulk of rigid walls.

To find an equation of state we need to write the conjugate variable for the volume parameter. This conjugated variable we will call *pressure parameter*, and it is found by derivation of the grand canonical potential

$$\Pi = -\left(\frac{\partial \Omega}{\partial \mathcal{V}}\right)_{T,\mu}, \tag{3.5}$$

what leads to

$$\Pi = \frac{(k_B T)^4}{\hbar^3} g_4(z), \tag{3.6}$$

and using this conjugated variable we can see that $\Omega = -\Pi\mathcal{V}$.

Now, we will describe a more realistic case, considering a fluid *with* interaction. The volume parameter, by definition, is not affected by considering the interaction between atoms, but the pressure parameter needs to be rewriten. In order to obtain Π we start to consider the grand partition function, defined in Equation 2.8 as

$$\mathcal{Z} = \sum e^{-\beta(H_N - \mu N)}$$

and now into the Hamiltonian of Equation 2.4 is inserted the interaction term: $H = K + U_{int} + U_{ext}$ with the kinetic energy given by $K = \sum_i \frac{P_i^2}{2m}$, and the interaction energy $U = \sum_{i<j} U(r_{ij})$. We will write the external potential as a harmonic oscillator $V_{ext} = \sum_i \frac{1}{2} m \left(\omega_x^2 x_i^2 + \omega_y^2 y_i^2 + \omega_z^2 z_i^2\right)$. The grand partition function is then

$$\mathcal{Z} = \exp\left[-\beta\left\{\sum_i \frac{P_i^2}{2m} + \sum_i \frac{1}{2} m \left(\omega_x^2 x_i^2 + \omega_y^2 y_i^2 + \omega_z^2 z_i^2\right) + \sum_{i<j} U r_{ij} - \mu N\right\}\right]. \tag{3.7}$$

Just to simplify the calculations, we can write the harmonic external potential in therms of the mean geometric frequency, $V_{ext} = \sum_i \frac{1}{2} m \left(\bar{\omega}^2 r_i^2\right)$, where $r_i^2 = x_i^2 + y_i^2 + z_i^2$. Then, using Equation 3.4, the external potential can be written in therms of the volume parameter $V_{ext} = \sum_i \frac{1}{2} m \mathcal{V}^{-2/3} r_i^2$, and Equation 3.7 becomes

$$\mathcal{Z} = \exp\left[-\beta\left\{\sum_i \frac{P_i^2}{2m} + \sum_i \frac{1}{2} m \mathcal{V}^{-2/3} r_i^2 + \sum_{i<j} U r_{ij} - \mu N\right\}\right]. \tag{3.8}$$

Using the definition of the pressure parameter, Equation 3.5,

$$\Pi = -\left(\frac{\partial \Omega}{\partial \mathcal{V}}\right)_{\mu,T}$$

and the relation between the grand canonical potential function and the grand potential, Equation 2.15, we write

$$\Pi = -\frac{1}{\beta}\frac{1}{\mathcal{Z}}\left(\frac{\partial \mathcal{Z}}{\partial \mathcal{V}}\right)_{\mu,T}, \tag{3.9}$$

and making the derivative of $\mathcal{Z}$

$$\left(\frac{\partial \mathcal{Z}}{\partial \mathcal{V}}\right)_{\mu,T} = -\frac{2\beta}{3\mathcal{V}} \sum_i \frac{1}{2} m \mathcal{V}^{-2/3} r_i^2 e^{-\beta(H_N - \mu N)}, \tag{3.10}$$

we obtain the pressure parameter

$$\Pi = \frac{2}{3\mathcal{V}}\frac{1}{\mathcal{Z}} \sum_i \frac{1}{2} m \mathcal{V}^{-2/3} r_i^2 e^{-\beta(H_N - \mu N)}. \tag{3.11}$$

Now, in order to obtain Π in a more convenient form, we can change from discrete to continuous writing

$$\sum_i \frac{1}{2} m \mathcal{V}^{-2/3} r_i^2 = \int d^3 r \frac{1}{2} m \bar{\omega}^2 r^2 \sum_i \delta(r - r_i), \tag{3.12}$$

which leads to

$$\Pi = \frac{2}{3\mathcal{V}} \int d^3r \frac{1}{2} m\bar{\omega}^2 r^2 \frac{1}{\mathcal{Z}} \operatorname{Tr}\left[\sum_i \delta(r - r_i) e^{-\beta(H_N - \mu N)}\right], \tag{3.13}$$

and since the density is given by

$$n\,(n) = \frac{1}{\mathcal{Z}} \operatorname{Tr}\left[\sum_i \delta(r - r_i) e^{-\beta(H_N - \mu N)}\right], \tag{3.14}$$

we finally obtain

$$\Pi = \frac{2m}{3\mathcal{V}} \int d^3r n(r) \left(\omega_x^2 x_i^2 + \omega_y^2 y_i^2 + \omega_z^2 y_i^2\right) \tag{3.15}$$

which is a very useful expression for the pressure parameter in terms of the cloud density and the external potential. This expression shows that the pressure parameter is obtained directly from the cloud analysis, since all quantities involved are easily measured with standard methods for extracting information of the clouds.

The pressure parameter depends on the density of the cloud, which is not homogeneous, and has two components for temperatures below T_c. These two components are well described by a Thomas-Fermi distribution (See Equation 2.47) for the condensed part and by a Gaussian distribution for the thermal part. The Thomas-Fermi distribution is given by

$$n_{BEC}\,(x, y, z) = n_{BEC}^0 \max\left[1 - \left\{\left(\frac{x}{R_x}\right)^2 + \left(\frac{y}{R_y}\right)^2 + \left(\frac{z}{R_z}\right)^2\right\}, 0\right] \tag{3.16}$$

where R_x, R_y, R_z are the BEC radii, and $n_{BEC}^0 = \frac{15 N_{BEC}}{8\pi R_x R_y R_z}$ is the peak density of the distribution which is found by the normalization condition for the number of condensed atoms $N_{BEC} = \int n_{BEC}(r) d^3r$.

In a similar way, the Gaussian distribution is given by

$$n_{th}\,(x, y, z) = n_{th}^0 \exp\left[-\frac{1}{2}\left\{\left(\frac{x}{\sigma_x}\right)^2 + \left(\frac{y}{\sigma_y}\right)^2 + \left(\frac{z}{\sigma_z}\right)^2\right\}\right] \tag{3.17}$$

where $n_{th}^0 = \frac{N_{th}}{(2\pi)^{3/2}\sigma_x\sigma_y\sigma_z}$ is the peak of the Gaussian distribution, N_{th} is the number of thermal atoms, and σ_x, σ_y, σ_z are the cloud widths (Gaussian function width).

Using the equations above, we evaluate Equation 3.15 and obtain the final equations for the two components of the pressure parameter,

$$\Pi_{BEC} = \frac{m N_{BEC}}{21\mathcal{V}} \left(\omega_x^2 R_x^2 + \omega_y^2 R_y^2 + \omega_z^2 R_z^2\right) \tag{3.18}$$

$$\Pi_{th} = \frac{mN_{th}}{3\mathcal{V}} \left(\omega_x^2\sigma_x^2 + \omega_y^2\sigma_y^2 + \omega_z^2\sigma_z^2\right). \tag{3.19}$$

We observe that the pressure parameter depends on the characteristics of the potential and the size of the cloud. The procedures to extract the number of atoms in each component, the widths of the thermal cloud, and the radii of the condensate will be described in Section 4.7.

The physical meaning of this parameter is discussed in references (36,40), where it is demonstrated that it has the same physical meaning that the local pressure of a fluid. The pressure parameter is related with the hydrostatic pressure by

$$\Pi\mathcal{V} = \int p(\vec{r})d^3r. \tag{3.20}$$

The last equation show us that although the pressure parameter does not have the same unit that the hydrostatic pressure, both have the same physical meaning, and also that we can find the pressure parameter from the hydrostatic pressure.

In Chapter 5, we will use this variables to evaluate the specific heat at constant volume for an ideal gas and we compare with the usual specific heat. Also, for an interacting system, we compare this variables with the local density approximation, and we will show that they are equivalent for the compressibility and for the equation of state.

4 Experimental setup

This chapter describes our experimental apparatus to produce Bose-Einstein condensation of ^{87}Rb atoms either in $|F = 2, m_F = 2\rangle$ or $|F = 1, m_F = -1\rangle$ states [*], and where this thesis has been developed. Some brief description can also be found in recent group's papers (43–44) and more details about the current version can be found in the master thesis. (48)

4.1 Experiment overview

There are many experimental configurations that are used to achieve Bose-Einstein condensation. The main goal is to capture the atoms at relatively high temperatures and taking them to very low temperatures, typically a few hundred nK, and densities on the order of $10^{14}\,\mathrm{cm}^{-3}$. Among many configurations, there is always a common requirement: the low background pressure required to achieve the condensation. The setup chosen by our group is the double-MOT (MOT - Magneto-Optical Trap) configuration (61), that is composed by two regions at different pressures, each one with an independent MOT.

The second chamber is built in order to obtain lower pressures, since the atoms source (dispensers) limits the pressure at about $10^{-9}\,\mathrm{Torr}$, which is not low enough to achieve Bose-Einstein condensation.

The atoms captured in the first MOT are continuously transferred to the second chamber, where again are captured in another MOT (named MOT2). The absence of the dispensers in the second chamber allows achieving very low pressures. In our experiment,

[*] Here F represent the hyperfine structure, that results from the coupling of the total angular momentum of the electron **J** with the total nuclar momentum (**I**). The label m_F represent the sublevels due the Zeeman effect for the hyperfine structure. For more details we recommend the reader to the reference (60).

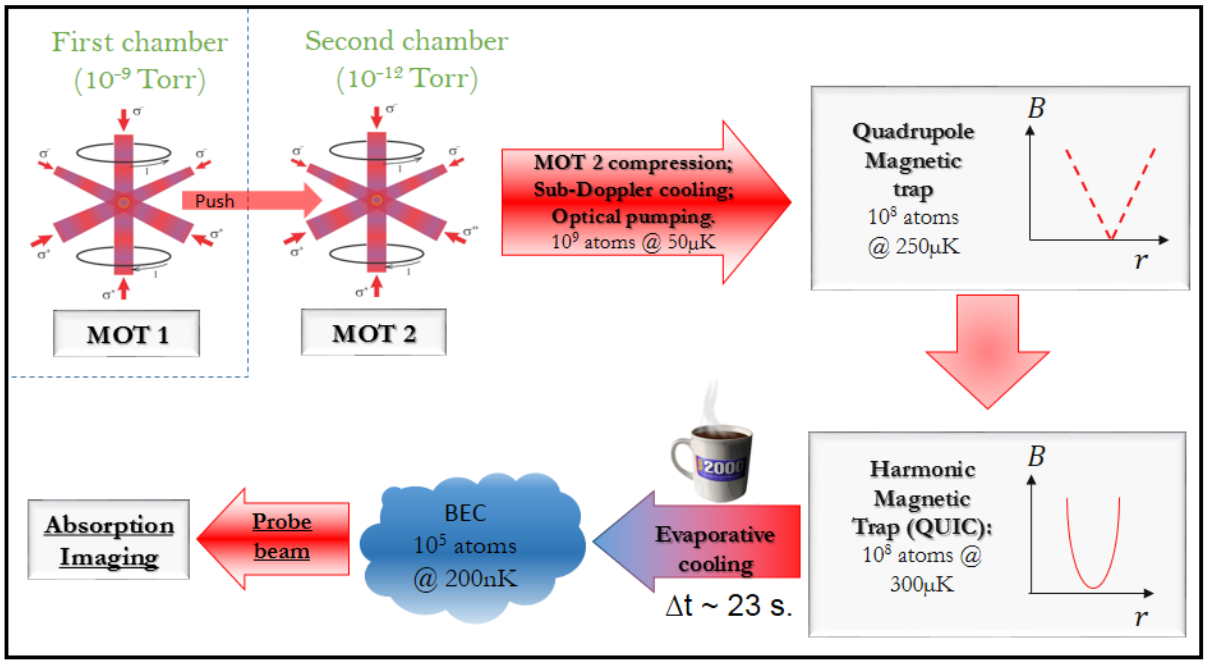

Figure 1 – Overview of the processes involved in the production of BEC in our experiment. Source: By the author.

this pressure is around 10^{-12} Torr, an ideal pressure to perform experiments in Bose-Einstein condensation.

The laser system is composed by three commercial diode lasers from TOPTICA ®Photonics (two DLX110L and one TA pro). They are electronically locked to a hyperfine line obtained from a saturated absorption spectroscopy signal. The frequency of these lasers is manipulated using acousto optic modulators to obtain other frequencies necessary for the experiment.

From the MOT to the condensation there are many steps needed to cool the atoms and to increase the phase space density. The main sequence used in our experiment is summarized in Figure 1. Basically, the atoms from the MOT2 are prepared in a sub-level magnetically trappable and then transferred to a magnetic harmonic trap, where we perform evaporative cooling and the BEC is produced.

To produce BEC there are many critical processes, where some microseconds are decisive in the reproducibility. To run the experiment we program a time sequence in a computer which controls all the analog and digital channels of two cards (National Instruments PCI 6259 and PXI 6733). The sequence is programmed using Python and

compiled with Labview, having a time precision of 5 μs, which means that is possible to generate pulses or ramps with duration as low as of 5 μs.

In what follows, we describe in more detail each one of these processes.

4.2 Vacuum system

The vacuum system is the first part to be built and one of the most important in the experiment. The goal in construct the vacuum system is to remove, as much as possible, the particles inside the chamber to avoid collisions with the trapped atoms. Once the high vacuum is reached the pressure is maintained the same for years, without any intervention.

To load a MOT, a pressure around 10^{-8} Torr is already enough, but this pressure does not allow the BEC achievement because at this pressure the losses by collisions with background vapor during the evaporative cooling overcome the increase in phase-space density. Using dispensers as the source of atoms to load the MOT limits the pressure in a value too high for studying Bose-Einstein condensation. A very common configuration, which solves this problem, is to build the system with two chambers, one to produce a first MOT and another one to make the other processes. This system is named as double-MOT configuration, and allows to reach low pressures.

Our system was built in this configuration and its three-dimensional representation is shown in Figure 2, which, in terms of pressure, can be differentiated in three regions: The MOT1 region, the differential pumping, and the science chamber. In the MOT1 chamber, the pressure is limited in 10^{-9} Torr, the second region, which is the connection between the two chambers, contain a narrow tube which provides the differential pumping between them. The third region is the science chamber and is kept at 10^{-12} Torr, that is already ultra-high-vacuum, ideal to produce and study BEC. Details about the construction and specifications can be found in reference. (48)

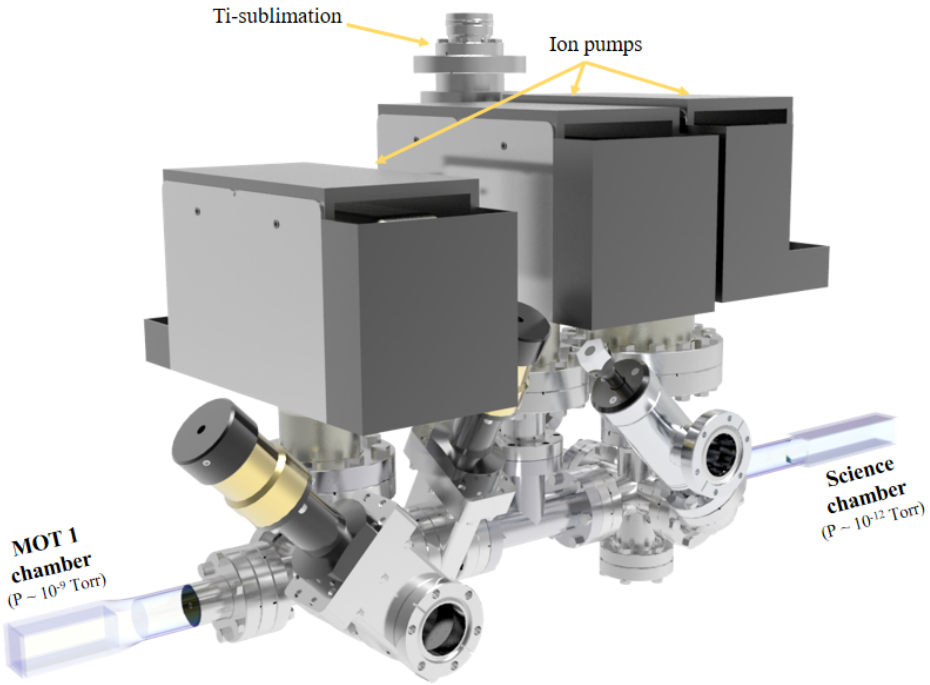

Figure 2 – Schematic drawing to the vacuum system. In the first chamber there are the dispensers, which are the atoms source for the experiment. In this chamber the atoms are trapped in a MOT which works as the atoms source for the science chamber. In the science chamber we perform all the other process required to obtain the condensation.

Source: By the author.

4.3 Double-MOT configuration

In the first chamber of our experiment there are the dispensers, which are the atoms source. It is a filament containing the atoms to be evaporated. The atoms are encapsulated with a reducing agent and the mixture is stable at room temperature but when it is heated at around 600 °C it spreads atoms. (62) The heating is usually done by means of an electric current, and the temperature of the dispenser is proportional to the current that flows through it. Typical values of current are between $1 \sim 6$ A.

The atoms released from the dispenser are trapped in a MOT. The MOT combines the radiation pressures of the laser with an inhomogeneous magnetic field and is able to confine about 10^9 atoms. The first realization of a MOT was in 1987 (18) and because it needs relatively weak magnetic field and power for the lasers, it became a very common choice to experiments in cold atoms.

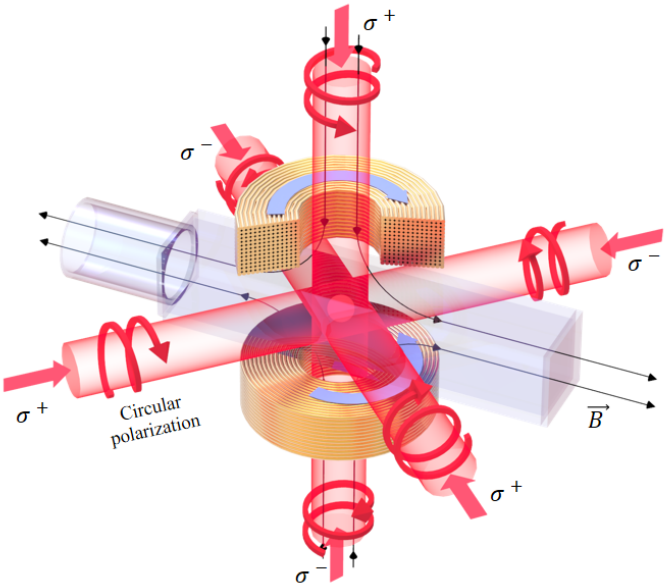

Figure 3 – Illustration for the magneto-optical trap configuration. The 3D-MOT is composed of three pairs (beams with opposite circularization) orthogonal counterpropagating laser beams and an inhomogeneous magnetic field produced by a pair of coils in anti-Helmholtz configuration.
Source: By the author.

A MOT is formed by three pairs of independent retro-reflected, circularly polarized, laser beams and a pair of coils in anti-Helmholtz configuration. Using an inhomogeneous magnetic field the energy levels of the atoms are shifted (Zeeman effect) and it makes the force experienced by their atoms dependent on the position and the frequency of the light. Figure 3 presents a representation of a MOT configuration, details and the theory about MOT and optical molasses can be found in references. (63–67)

The frequency of the trap beams is red-detuned with the $5S_{1/2}(F = 2) \rightarrow 5P_{3/2}(F = 3)$ transition to cool the atoms rather than heat them. Also, when this detuning is combined with the correct polarization and magnetic field gradient creates the restoring force that confine the atoms.

Another beam is necessary to recover the atoms that occasionally decay to the $(F = 1)$ state. This light, called repumper light, is superimposed with the trap beams and is resonant with the $5S_{1/2}(F = 1) \rightarrow 5P_{3/2}(F = 2)$ † transition.

† Here we are using the spectroscopic notation in which the atomic state is labeled by $^{2S+1}L_J$. Using this notation, the orbital angular momentum $(L = 0, 1, 2, 3, ...,)$ is associated with the a letter $(S, P, D, F, ...,)$. S and J are the spin angular momentum and the total angular momentum of the electron respectively. We recomend the reference (60) for more details.

The magnetic gradient field for the MOT does not have to be intense, about 10 G/cm is enough, and is generated by two coils in anti-Helmholtz configuration. Three additional pairs of coils are orthogonally positioned to change the position of the MOT and to help better transfer them to the second chamber. Using a total power of about 100 mW for the trap beams and around 25 mW for the repumper, the MOT1 traps around 3×10^8 atoms with a temperature of $\sim 320\,\mu$K.

The atoms in the MOT1 are the source for the MOT2 and are continuously transferred to the second chamber by a beam (push beam) with 2 mW of power resonant with the trap transition of the MOT1. In the second chamber the atoms are captured by another magneto-optical trap. This trap is similar to the MOT1, the difference is that the beams for the MOT2 are totally independent instead of being retro-reflected, since this gives more control to transfer the atoms to the magnetic trap. The MOT2 traps about 2×10^9 atoms at the same temperature of the MOT1, and it is necessary 30 s to fully load this MOT. Once the MOT2 is loaded, the atoms are transferred to a pure magnetic trap where it will be performed evaporative cooling. Some procedures need to be done to efficiently transfer the atoms from the MOT to the magnetic trap and they will be described in the next section.

4.4 Transference to the magnetic trap

This MOT to magnetic trap transference is very critical for some reasons that we will discuss here, and the main goal is to optimize the number of atoms loaded in the magnetic trap and its phase space density. The higher the number of atoms and the lower the temperature after these processes will maximize the efficiency in the evaporative cooling.

During the transference , the cloud size and its position are very important . The position of the quadrupole trap center is fixed by the position of the coils, and the cloud

position needs to match the trap center to avoid heating. The position of the cloud can be set by the alignment of the beams, but it is also easier to transfer smaller clouds. We make the following sequence to maximize this transference and to prepare the cloud before evaporative cooling.

The first step is a compression of the cloud, which was first demonstrated by Petrich *et al* in 1994. (68) In this process the frequency of the cooling laser is red detuned to decrease the photon scattering rate and make the atoms accumulate in the trap center, reducing the cloud size. There is the possibility to make this process at the same time of an increasing in the magnetic field gradient. In our experiment we found the best parameters changing the detuning frequency from $\Delta = -20\,\mathrm{MHz}$ to $\Delta = -60\,\mathrm{MHz}$ in $5\,\mathrm{ms}$ and it makes no difference in changing the magnetic field gradient, which remains fixed during this process.

The next step, known as optical molasses or sub-Doppler cooling (69), is used to decrease the temperature of the cloud. The magnetic field is switched off and the cloud expands in the presence of light, whose frequency again is shifted further from the transition. The power in this process is naturally decreased by the efficiency of the modulators when the frequency is set far from the value where they are optimized. In the experiment the frequency is shifted to $-70\,\mathrm{MHz}$ and the cloud expands for $4\,\mathrm{ms}$. The final temperature of the cloud after this process is around $50\,\mu\mathrm{K}$.

Finally, when all the processes to decrease the temperature of the cloud and to increase its density are finished, the atoms have to be prepared in a state magnetically trappable. After the optical molasses, the atoms are in a mixture of all the five Zeeman states of the $F = 2$, and only two of them are magnetically trappable. Because of its higher magnetic moment, the $|F = 2, m_F = 2\rangle$ has stronger confinement in magnetic traps, which makes easier the process of evaporative cooling. Since the first version of this experiment the $|F = 2, m_F = 2\rangle$ state has been chosen for all research topics, but recently, in a study by our group involving quantized vortices in BEC, the $|F = 1, m_F = -1\rangle$ became an option to generate vortices with different charges.

To choose between the two states, the optical pumping process needs to be different

to make it efficient in transfer the atoms into the desired state. Both states need to be optically pumped with pulses of circularly polarized light, since it makes transitions between the m_F and $m_{F\pm1}$ state. Two pulses of light resonant with a defined transition are applied to increase the probability that the atom will be in the desired state after the optical transitions.

When we select the $|F = 2, m_F = 2\rangle$ state, we make a pre-optical pumping switching off the trap light 0.5 ms before the repumper light, and it places most of the atoms in the $F = 2$ manifold. After this, we apply a homogeneous magnetic field of about 1 G which split the Zeeman levels. The efficiency in populating the $|F = 2, m_F = 2\rangle$ state has a maximum in about 70 % when two pulses of right-circular polarized light are applied, one is resonant with the $5S_{1/2}(F = 1) \rightarrow 5P_{3/2}(F = 2)$ transition and the other is set in the $5S_{1/2}(F = 2) \rightarrow 5P_{3/2}(F = 2)$ transition. The first pulse $(1 - 2)$ stays on for 120 μs, and the second one $(2 - 2)$ for 25 μs.

In order to populate the $|F = 1, m_F = -1\rangle$, the pre-optical pumping is done switching off the repumper light 0.5 ms before the trapping light to place most of atoms in the $F = 1$ manifold. After this, we need to apply left-circular polarized light in the atoms to induce $m_F \rightarrow m_{F-1}$ transitions. We turn on the homogeneous magnetic field to split the Zeeman states and then we apply two pulses of left-circularly polarized light, one of them resonant in the $5S_{1/2}(F = 1) \rightarrow 5P_{3/2}(F = 1)$ transition, with duration of 80 μs and the other one in the $5S_{1/2}(F = 2) \rightarrow 5P_{3/2}(F = 2)$ transition which stays on for 1.2 ms. Following this procedure the efficiency in transfer the atoms to the $|F = 1, m_F = -1\rangle$ state is about 50 %.

After the optical pumping process all the light in the science chamber is turned off and the atoms are prepared to be caught in the pure magnetic trap.

4.5 Magnetic trap

Magnetic traps work due to the interaction of the magnetic moment $\overrightarrow{\mu}$ of an atom with a magnetic field $\overrightarrow{B}$. The potential energy of this interaction is given by $V = \overrightarrow{\mu} \cdot \overrightarrow{B} = m_F g_F \mu_B |\overrightarrow{B}|$, where m_F is the Zeeman level, g_F is the Landé g-factor, and μ_B is the Bohr magneton.

The energy interaction between the atom and the magnetic field depends on the atom state. For ^{87}Rb, $g_f = -1/2$ for the $F = 1$ state and is $g_f = 1/2$ for $F = 2$. So, the energy of the states $|F = 2, m_F = 2\rangle$, $|F = 2, m_F = 1\rangle$ and $|F = 1, m_F = -1\rangle$ increase as the magnetic field increases, what makes them "*low-field seekers*". The states whose energy decreases as the magnetic field increases are known as "*high-field seekers*". By creating a trap with a minimum in the magnetic field it is possible to capture the "*low-field seekers*".

Between all the three magnetically trappable states the $|F = 2, m_F = 2\rangle$ has the strongest interaction with the magnetic field, and since for this state the trap is tighter, this is the most favorable to be condensed through the magnetic evaporative cooling process.

We capture the atoms in a magnetic trap after the optical pumping process by increasing the current in the quadrupole coils. The magnetic field is increased, from about 20 G/cm used in the MOT, to 75 G/cm in a few milliseconds, optimized to capture the largest number of atoms.

After capturing the atoms, we increase the gradient to a value which allows an effective collision rate for evaporative cooling. This increasing is performed to a final value of 330 G/cm in a linear ramp of 400 ms and it remains fixed to the end.

Advantages in magnetic quadrupole traps include its high efficiency in capture the atoms from the MOT, due to its large trapping volume, the inconvenient is that its minimum is a point with zero magnetic field, and for "*low-field seekers*" this is the point where it minimizes the energy, and where they are susceptible to suffer a change for a non-trappable state, known as Majorana spin flips (70) which push the atoms outside the

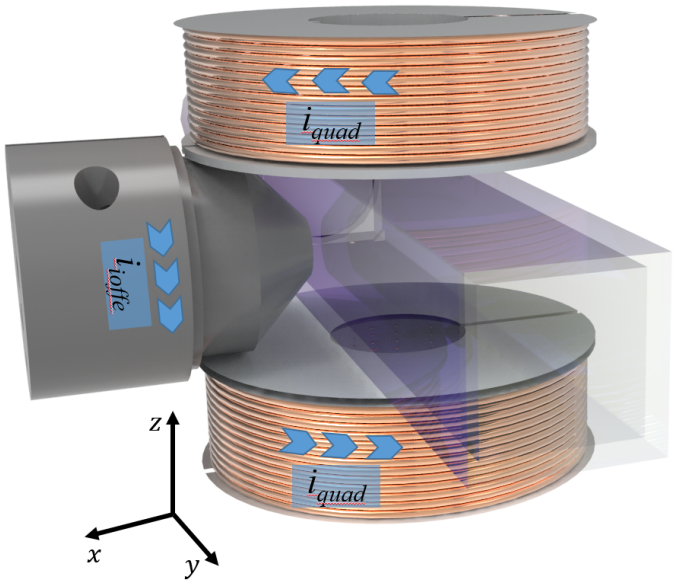

Figure 4 – Illustration for QUIC trap configuration used in our experiment. The QUIC trap is formed by a pair of coils in anti-Helmholtz configuration (quadrupole coils) and another coil (Ioffe) which transforms the minimum (which is zero) for the quadrupole potential into a harmonic potential with a non-zero minimum.
Source: By the author.

trap.

To solve this inconvenient some solutions were implemented using blue detuned laser (23), red detuned lasers (71), and using other configurations for the magnetic field. (72–74) The last reference uses a single coil (Ioffe coil) perpendicular to the quadrupole axis which, combined with the quadrupole field, results in a harmonic potential. This configuration is known as Quadrupole-Ioffe configuration (QUIC) and was adopted in our system. The correspondent drawing is presented in Figure 4.

The quadrupole and Ioffe coils are in series connected and the conversion from the quadrupole trap to harmonic QUIC trap is done by slowly increasing the current in the Ioffe. The time duration for this conversion is 600 ms and, as can be observed in Figure 5, when the current in the Ioffe has almost the same value of the quadrupole current, the potential has a harmonic profile which can be described as

$$V(x,y,z) = V_0 + \frac{m}{2}\left(\omega_x^2 x^2 + \omega_y^2 y^2 + \omega_z^2 z^2\right) \quad , \tag{4.1}$$

where V_0 is the non-zero potential minimum value (this minimum value is proportional to

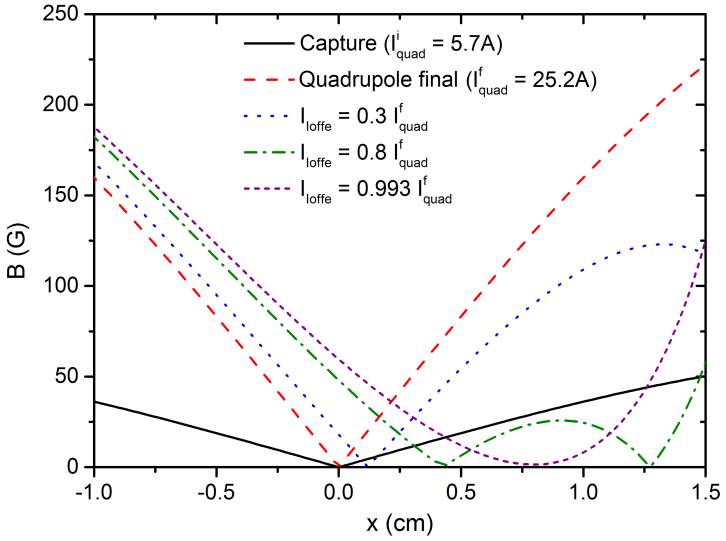

Figure 5 – Magnetic field magnitude in the Ioffe direction (x-direction of Figure 4) for a few values of current in the Ioffe coil. Increasing the current in the Ioffe to almost the same as the current in the quadrupole coils, the field becomes harmonic.
Source: By the author.

a magnetic field of about 1.4 G). The theoretical values for the frequencies are given by

$$\omega_r = \sqrt{\frac{m_F g_F \mu_B}{m} \frac{(B'_r)^2}{B_0}}, \qquad \text{and} \qquad \omega_z = \sqrt{m_F g_F \mu_B B''/m},$$

where m is the atomic mass, B_0 is the minimum value of the magnetic field, B' is the gradient in the radial direction and B'' is the curvature (75). The values B_0, B', e B'' are given by the coils geometry and the current through them. In our experiment the maximum current is 25 A and for this value we obtain $B_0 = 1.22$G, $B'_z = 162$G/cm, $B'_r = 165$G/cm, and $B''_z = 282.8$G/cm^2. Using these parameters we can calculate the frequencies for the trap which depend on the m_F state. We obtain $\omega_x = \omega_y = \omega_r = 2\pi \times 190.5$Hz and $\omega_z = 2\pi \times 21.4$Hz for the $|F = 2, m_F = 2\rangle$ and for $|F = 1, m_F = -1\rangle$ we obtain $\omega_r = 2\pi \times 137.7$Hz and $\omega_z = 2\pi \times 15.2$Hz

The frequencies of the trap can be measured by exciting the condensate dipolar mode, which can be done by modulating the magnetic field. The measured frequencies for our experiment are given by $\omega_x = 2\pi \times 21$ Hz, $\omega_y = 2\pi \times 189$ Hz and $\omega_z = 2\pi \times 187$ Hz, for the $|F = 2, m_F = 2\rangle$ states and $\omega_x = 2\pi \times 15$ Hz, $\omega_y = 2\pi \times 133$ Hz and $\omega_z = 2\pi \times 134$ Hz for the $|F = 1, m_F = -1\rangle$ state. All of them are very close to the expected theoretical values.

After all these process we obtain $\sim 4{\times}10^8$ atoms at about 450 μK and $\sim 2.5{\times}10^8$ atoms

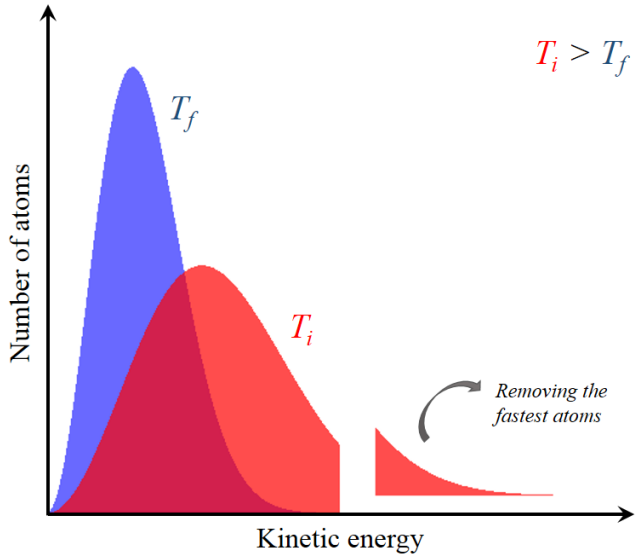

Figure 6 – Representation of the evaporative cooling process. When the most energetic atoms are removed from the trapping potential, the atomic sample retermalizes and its temperature decreases.
Source: By the author.

at about 250 μK for the states $|F = 2, m_F = 2\rangle$ and $|F = 1, m_F = -1\rangle$ respectively. The next step is to cool the atoms using evaporative cooling to achieve the condensation.

4.6 Evaporative cooling induced by radio-frequency

Atoms or molecules in a gas have an atomic velocity distribution well described by the Maxwell-Boltzmann distribution. Evaporative cooling is the process of removing the most energetic atoms (hottest atoms) from the ensemble, allowing the remaining atoms to rethermalize in a lower temperature by elastic collisions. A representation of this process is shown in Figure 6.

Evaporative cooling of trapped atoms was first proposed in 1985 to cool spin-polarized hydrogen (10), and the first demonstration was done in 1988 (11). Evaporative cooling works in a competition between cooling and lifetime of the sample: For an efficient process the thermalization must allow decreasing the temperature in a time shorter than

the lifetime of the cloud inside the trap.

In 1989 (21) this technique receives its major improvements: The proposal was to use radio frequency (RF) radiation to remove atoms in a selective way. The first demonstration of forced evaporative cooling using RF was reported in 1993 (76) and it proved to be effective in increasing the phase-space density. The radio frequency changes the atomic state taking them to a non-trappable state, expelling the atoms from the trap.

This technique has high efficiency in selective removal of atoms because the energy between two Zeeman levels is proportional to the magnetic field. The most energetic atoms will fell higher magnetic fields, consequently, the resonant frequency can be set to remove only the most energetic atoms without affecting the colder atoms. A more detailed discussion about evaporative cooling in magnetic traps can be found in reference (77) and here we will discuss just the procedure followed in our experiment.

In our experiment, the separation between the Zeeman levels is about 20 MHz for the hottest atoms, defining the appropriate value to start the evaporation. To find the exact value we turn on the RF when the atoms are in the QUIC trap and we keep it on for some time, starting with high values of RF and decreasing this value observing the number of atoms remaining in the trap. When the RF affects the most energetic atoms they are removed from the trap and then we know the value of RF for starting the evaporative process.

Starting with this value we need to optimize the evaporation in order to reach the condensation, which occurs only if the phase space density (PSD) is greater of equal to 2.612. The efficiency of the evaporation is determined by the number of atoms which remain at the end of the process. In this way, evaporation needs to be performed with a maximum increase in phase-space density with the smallest loss in the number of atoms. In this process, when the hottest atoms are removed, the collisions between atoms allow the rethermalization of the cloud in a lower temperature. The objective is to make a runaway evaporation, which consists in decreasing the temperature, keeping constant or increasing the collision rate.

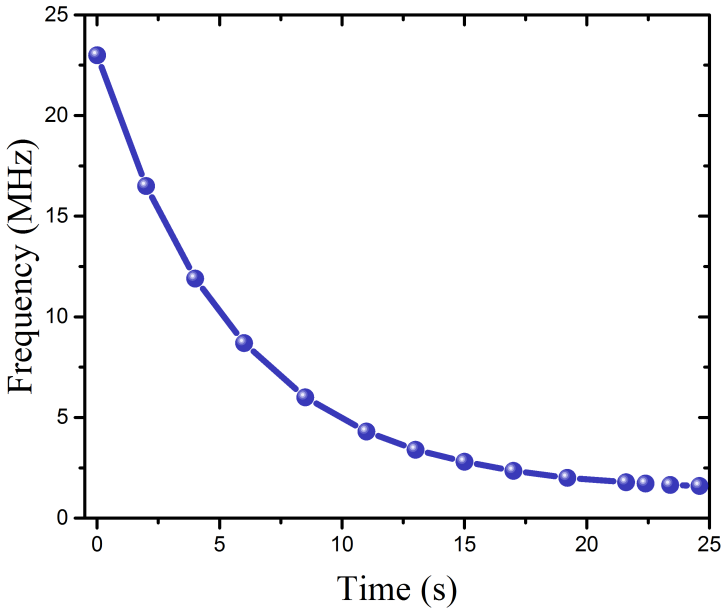

Figure 7 – Experimental evaporation ramp applied in the atoms to reach the condensation. The ramp is broken in small ramps to improve the optimization. The best final ramp presents a typical exponential curve.
Source: By the author.

After a good and detailed discussion about all the relevant quantities in the evaporation process, Ketterle (77) point that since the goal is to increase the phase space density, the best parameter to be optimized is given by

$$\gamma = \frac{\ln(PSD_{final}/PSD_{initial})}{\ln(N_{final}/N_{initial})}. \tag{4.2}$$

To improve the efficiency, we break the RF ramp in many other linear ramps, and for each one we optimize γ. These small ramps are defined with an initial and a final frequency and the velocity for this swap is optimized to find the best γ. After optimized the first section we add a new one and we repeat the process. The entire ramp is shown in Figure 7, and it is possible to observe an exponential behavior starting in 23 MHz and finishing in 1.6 MHz. In fact, after we have found the frequency to start the evaporation, one exponential ramp is sufficient to reach the condensation, and the only parameter to be optimized is the time constant of the exponential function.

As discussed in the previous section, the processes used to increase the PSD before the transference to the QUIC trap are more efficient for the $F = 1$ than for the $F = 2$. On the other hand, in forced evaporative cooling, the potential is stronger for the $F = 2$, which makes the rethermalization faster, resulting in a shorter time to achieve the degeneracy. In

our experiment, the duration for evaporation of either state are almost the same, because for the $F = 1$ the cloud is a lot colder, consequently, the variation in the temperature required to achieve the condensation is smaller.

After evaporative cooling, we obtain an almost pure BEC of around 2×10^5 atoms in the $|F = 2, m_F = 2\rangle$ or around 3×10^5 atoms in the $|F = 1, m_F = -1\rangle$.

In the following section, we describe the last step of the experiment, which consists in imaging the atoms to obtain all the relevant information.

4.7 Probing the atoms

In our experiment, we use absorption image to obtain all information about the atom cloud. In this technique, a resonant probe beam is used to illuminate the cloud and its shadow is imaged in a camera CCD. The image profile is then analyzed and it provides the quantities such as atom number, dimensions of the cloud, temperature, and phase-space density. Since the cloud is too dense to be imaged in trap, the atoms are released and allowed to freely expand before probing, what is known as time-of-flight (TOF).

4.7.1 Imaging

For absorption image it is necessary to have a normalized image constructed from three different images. The first image (atoms) is taken with the atoms to obtain its shadow. The second image (probe) is taken without atoms to capture the intensity of the probe, and finally, the third one (background) is taken without any light in the experiment, which gives information about the background level.

We make all pulses with $40\,\mu$s with power about $800\,\mu$W. The CCD, triggered

and synchronized by the computer control, capture the intensity of each image and send it to a computer which makes the normalization: $I_N = (I_{atoms} - I_{background})/(I_{probe} - I_{background})$. The normalized image I_N will provide the density profile of the cloud which is then analyzed to extract relevant information. The absorption of the probe light is well described by the Beer's law

$$I(x,y) = I_0(x,y)e^{-OD(x,y)} \quad , \tag{4.3}$$

where $I(x,y)$ is the intensity of the light propagating along the z direction, $I_0(x,y)$ is the initial probe beam intensity, $OD(x,y) = \sigma_0 \int n(x,y,z)dz$ is the optical density distribution of the sample and σ_0 is the absorption cross-section (for ^{87}Rb, $\sigma_0 \approx 1.36 \times 10^{-9}\,\mathrm{cm}^2$ (78)).

From Equation 4.3 we obtain

$$OD(x,y) = -\ln\left(\frac{I(x,y)}{I_0(x,y)}\right), \tag{4.4}$$

which is the optical density profile of the cloud. The quantity $\frac{I(x,y)}{I_0(x,y)}$ is exactly the result of the normalized image and is used to extract information of the cloud. The optical density profile of the normalized absorption image is fitted by the theoretical distribution which is defined according to the characteristic of the cloud (thermal or condensed). The routine is programmed in a computer using Python, and soon after the image is received on the computer all the calculations are done and the information is available.

In the following, we describe the theoretical functions that are used to extract information of the cloud.

4.7.2 Fitting

In section 2.2 we found the density distribution of a Bose-Einstein condensate making the Thomas-Fermi approximation. For a harmonic trapping potential the density distribution $n_{TF}(x,y,z)$ for the cloud has a parabolic profile (See Equations 2.44 and 3.16). The absorption image is the integration of this distribution in the probe direction,

what results in a 2D density distribution given by

$$OD_{TF}(x,y) = OD_{TF}^{peak} \max\left[\left(1 - \frac{(x-x_0)^2}{R_x^2} - \frac{(y-y_0)^2}{R_y^2}\right)^{3/2}, 0\right] \tag{4.5}$$

where OD_{TF}^{peak} is the peak value of the distribution, x_0 and y_0 are the center of mass coordinates. For thermal cloud the density distribution is described by the classical Maxwell-Boltzmann distribution (See Equation 3.17). In this way, we can fit the thermal cloud by a Gaussian function

$$OD_{th}(x,y) = OD_{th}^{peak} \exp\left[-\frac{(x-x_0)^2}{\sigma_x^2} - \frac{(y-y_0)^2}{\sigma_y^2}\right] \tag{4.6}$$

where OD_{TF}^{peak} is the peak value of the distribution.

When the cloud is partially condensed, i.e. below the critical temperature, there are thermal and condensed atoms, and to extract the information we need to fit it with an appropriate function that we call bimodal function, which is the sum of Gaussian and Thomas-Fermi functions defined above. Using the optical density for each part, we write the bimodal optical density of the cloud as $OD_{bim}(x,y) = OD_{TF}(x,y) + OD_{th}(x,y)$.

The number of thermal atoms can be obtained by integrating the thermal density,

$$N_{th} = \int n_{th}(x,y,x)dxdydz = \frac{1}{\sigma_0}\int OD_{th}(x,y)dxdy, \tag{4.7}$$

which results in

$$N_{th} = \frac{2\pi OD_{th}^{peak}}{\sigma_0}\sigma_x\sigma_y, \tag{4.8}$$

and by integrating the condensate density we obtain the number of condensed atoms

$$N_{BEC} = \frac{2\pi OD_{TF}^{peak}}{5\sigma_0}R_xR_y. \tag{4.9}$$

The temperature of the cloud can be obtained by the expansion of the cloud in TOF since the cloud expands freely. The expansion velocity (v) is constant and related to the temperature through the expression

$$\frac{1}{2}k_BT = \frac{1}{2}mv^2, \tag{4.10}$$

where m is the mass of the atoms. When the cloud is released from the trap, its width in each direction (i) will increase linearly, and after a time t (which is the time-of-flight), $\sigma_i^2 = \sigma_{i0}^2 + v_i^2 t^2$. After a large time-of-flight[‡] we can assume $\sigma_{i0} \ll \sigma_i$, resulting in

$$T = \frac{m}{k_B}\left(\frac{\sigma}{t}\right)^2. \tag{4.11}$$

[‡] for a harmonic trap this condition is valid when $t > 1/\omega_i$, where ω_i is the frequency of the trap in the i direction.

5 Comparison between global variables and other approaches

An inconvenient to study thermodynamics in trapped Bose gases is that the usual variables are not always good variables to study this system. We are familiarized to work with the usual equation of state for a gas in a bulk of rigid walls, where we can directly define pressure and volume. However, Bose-Einstein condensates are produced in trapping potentials where the trap interacts with the gas everywhere, what leads us to make considerations about the volume and pressure. If we consider a thermal cloud in a harmonic trapping potential, its density has a Gaussian profile, and is not possible to define a finite space for the volume occupied by the cloud.

Other inconvenient is that most of the traps where BEC is achieved are harmonic, and this leads to a non uniform density profile. With such a versatile system to test many fields of physics, there are not many studies involving thermodynamics in trapped gases, and this comes from the difficulty to obtain valid thermodynamic parameters, such as volume and pressure. Some properties of the gas can be measured by using the local density approximation (LDA), which consist in consider that locally the density, or the potential, can be considered uniform. One important work where the LDA is applied was published by a group at MIT (35), where they used this theory to study thermodynamics on a Fermi gas.

One alternative is to use the global variables, which were defined specifically for these systems. These variables have been used in our group to study thermodynamics in trapped gases, and they have presented the typical behavior that is expected to be observed with the conventional treatment. In every work where global variables are used, it is difficult to compare with other approaches because these variables do not have the same usual meaning, and the analogy needs to be done with attention. For this reason, only qualitative comparisons were done until now.

In this chapter, we theoretically test the validity of the global thermodynamic variables by comparing it, as much as possible, with other methods.

For an ideal gas we compare the specific heat evaluated using the global variables with that evaluated using the standard statistic treatment. We use the simplicity to obtain an expression for the *interacting* gas in the global approach, to see the effects of the interaction in the specific heat.

Then, for the same interacting system we use the local-density approximation to obtain expressions for the compressibility and the equation of state. We used the global variables to obtain equivalent expressions and then we make a comparison between both methods.

5.1 Specific heat for an ideal gas: Conventional versus global variables

5.1.1 Conventional specific heat

The specific heat for an ideal gas is vastly discussed in standard books of thermodynamics and statistical mechanics, and is obtained by first writing the energy, and then deriving it with respect to the temperature. We will call this procedure *conventional* specific heat.

By definition, the specific heat is given by

$$C_V = \left(\frac{\partial E}{\partial T}\right)_V . \tag{5.1}$$

For an ideal Bose gas, the internal energy is obtained by summing the energy of all states,

$E = \sum_j \epsilon_j n_j$. With n_j given by Equation 2.18,

$$n_j = \frac{1}{\exp\left[\beta(\epsilon_j - \mu)\right] - 1}, \tag{5.2}$$

we obtain

$$E = \sum_{j=0}^{\infty} \frac{\epsilon_j}{\exp\left[\beta(\epsilon_j - \mu)\right] - 1}. \tag{5.3}$$

In a BEC we have two important regimes of temperature, these regimes are defined by the transition where the condensation takes place. Above the critical temperature there is only thermal component, and consequently, we need to compute only the energy of thermal atoms. Below the critical temperature condensed atoms also are present, and we need to analyze its fraction as a function of temperature.

We start evaluating the energy for the condensed phase. In this regime we need just to evaluate the energy of the excited atoms, since the energy of the condensate is zero, as well as the chemical potential for non interacting particles. In the last equation, since the condensed atoms do not contribute for the total energy, we can simple convert the sum into an integral without an additional term, what leads to

$$E = \frac{1}{2(\hbar\bar{\omega})^3} \int_0^{\infty} \frac{\epsilon^3}{\exp(\beta\epsilon) - 1} d\epsilon, \tag{5.4}$$

which, after using the integral

$$\int_0^{\infty} \frac{x^{n-1}}{e^x - 1} dx = \Gamma(n)\zeta(n) \tag{5.5}$$

results in

$$E = \frac{1}{2\beta^4(\hbar\bar{\omega})^3}\Gamma(4)\zeta(4) = \frac{1}{2(\hbar\bar{\omega})^3}\Gamma(4)\zeta(4)(k_B T)^4. \tag{5.6}$$

In order to write the energy as a function of the number of atoms and the critical temperature, we can use Equation 2.31

$$T_c = \frac{\hbar\bar{\omega}}{k_B}\left(\frac{2N}{\Gamma(3)\zeta(3)}\right)^{1/3}, \tag{5.7}$$

which allows us to rewrite the energy. After replacing the last expression, we obtain

$$E = 3Nk_B \frac{\zeta(4)}{\zeta(3)} \frac{T^4}{T_c^3}. \tag{5.8}$$

Finally, after finding the equation for the energy, we derive it with respect to T to obtain the specific heat at constant volume for the condensed phase,

$$C_V^{BEC} = 12Nk_B\frac{\zeta(4)}{\zeta(3)}\left(\frac{T}{T_c}\right)^3. \tag{5.9}$$

To find the expression for the specific heat valid above and close of T_C we need to expand the exponential term in the expressions for the number of atoms and the energy. (54) This expansion can be done because at higher temperatures the exponential term, which is proportional to T^{-1}, becomes small.

Using the expansion $(e^x - 1)^{-1}$ in the general expression for the number of thermal atoms, Equation 2.23, and for the energy , Equation 5.4 with $\mu \neq 0$, we obtain

$$N \simeq \frac{1}{2(\hbar\bar{\omega})^3}\int_0^\infty \epsilon^2\left[e^{\beta(\mu-\epsilon)} + e^{2\beta(\mu-\epsilon)}\right]d\epsilon, \tag{5.10}$$

and

$$E \simeq \frac{1}{2(\hbar\bar{\omega})^3}\int_0^\infty \epsilon^3\left[e^{\beta(\mu-\epsilon)} + e^{2\beta(\mu-\epsilon)}\right]d\epsilon. \tag{5.11}$$

From these two expressions, and using Equation 2.31 for the critical temperature, we obtain

$$E \simeq 3NK_BT\left[1 - \frac{\zeta(3)}{16}\left(\frac{T_c}{T}\right)^3\right], \tag{5.12}$$

and then

$$C_V^{th} \simeq 3NK_B\left[1 + \frac{\zeta(3)}{8}\left(\frac{T_c}{T}\right)^3\right]. \tag{5.13}$$

Analyzing this expression for very high temperature we obtain

$$C_V^{th} = 3NK_B, \tag{5.14}$$

that is the known result for the specific heat of an ideal gas.

The last expression can also be obtained if we consider that at higher temperatures the occupation number becomes small and the Bose-Einstein distribution reduces to the Maxwell-Boltzmann distribution ($e^{\beta(\epsilon-\mu)} \gg 1$), what leads to the number of atoms and the energy to be written as

$$N = \frac{1}{2(\hbar\bar{\omega})^3}\int_0^\infty \epsilon^2 e^{\beta(\mu-\epsilon)}d\epsilon, \tag{5.15}$$

and

$$E = \frac{1}{2(\hbar\bar{\omega})^3}\int_0^\infty \epsilon^3 e^{\beta(\mu-\epsilon)}d\epsilon, \tag{5.16}$$

respectively.

After making an integration by parts of Equation 5.16 we obtain

$$E = \frac{1}{2(\hbar\bar{\omega})^3}3k_BT\left[\int_0^\infty \epsilon^2 e^{\beta(\mu-\epsilon)}d\epsilon\right]. \tag{5.17}$$

The term in brackets is the equation for the number of atoms, then the energy is given by

$$E = 3Nk_BT, \tag{5.18}$$

and consequently the specific heat for the thermal part is

$$C_V^{th} = 3Nk_B. \tag{5.19}$$

5.1.2 Global specific heat

The energy is the fundamental part to obtain the specific heat. Using global variables, the internal energy of a trapped gas in a harmonic trap is $E_{th} = 3\Pi_{th}\mathcal{V}$ for the thermal atoms and $E_{BEC} = \frac{5}{2}\Pi_{BEC}\mathcal{V}$ for the condensate. (41) The energy for the thermal part is easily obtained if we write the internal energy following the derivation of Equation 2.27, the difference is just that the energy is given by $E = \sum_j \epsilon_j n_j$ and the number of atoms is just $N = \sum_j n_j$.

If we follow the same procedures we will obtain that the internal energy for a thermal cloud is given by

$$E_{th} = \frac{1}{2\beta^4(\hbar\bar{\omega})^3}g_4(z)\Gamma(4), \tag{5.20}$$

and using Equations 3.4 and 3.6, and the numerical value $\Gamma(4) = 6$ we direct obtain that $E_{th} = 3\Pi\mathcal{V}$.

We can separate the pressure parameter in thermal and BEC parts, in other words, $\Pi = \Pi_{th} + \Pi_{BEC}$ what allow us to write

$$E = 3\Pi_{th}\mathcal{V} + \frac{5}{2}\Pi_{BEC}\mathcal{V} = 3\Pi\mathcal{V} - \frac{1}{2}\Pi_{BEC}\mathcal{V}. \tag{5.21}$$

Now we can obtain the specific heat at constant *volume parameter* as $C_{\mathcal{V}} = \left(\frac{\partial E}{\partial T}\right)_{N,\mathcal{V}}$. The energy of the condensate is almost irrelevant for the specific heat since $\left(\frac{\partial \Pi_{BEC}}{\partial T}\right) \ll \left(\frac{\partial \Pi_{th}}{\partial T}\right)$. In our experiment $\left(\frac{\partial \Pi_{BEC}}{\partial T}\right) / \left(\frac{\partial \Pi_{th}}{\partial T}\right) < 0.1$ even for the lowest temperatures. By neglecting the last therm of Equation 5.21 we find that the approximated specific heat is given by

$$C_{\mathcal{V}} = 3\mathcal{V}\left(\frac{\partial \Pi}{\partial T}\right)_{N,\mathcal{V}}. \tag{5.22}$$

5.1.3 Comparison

Global variables were defined in Chapter 3 and we have obtained expressions for the pressure parameter either for an interacting or non interacting systems. Also, we have shown in Equation 5.22 that the specific heat is proportional to a derivative of the pressure parameter with the temperature.

Since the pressure parameter is different for an ideal and an interacting system, we will first consider the ideal gas that is the simplest case, then we treat a more realistic case considering the interaction.

For an ideal gas, i.e. *without* interaction, the global variables must provide the same results that the conventional statistical treatment. This is clear if we look at the beginning of Chapter 3, where we have introduced the global variables. We *defined* the volume parameter after making the standard statistical treatment to find the grand canonical potential Ω, and see that Ω is proportional to the inverse of the frequencies of the trapping potential.

By writing the pressure parameter for an ideal gas (Equation 3.6)

$$\Pi = \frac{(k_B T)^4}{\hbar^3} g_4(z),$$

and deriving it with respect to temperature to find the specific heat (See Equation 5.22) we will find

$$C_{\mathcal{V}} = 12\mathcal{V}\frac{k_B^4 T^3}{\hbar^3} g_4(z), \tag{5.23}$$

which is equivalent to the expression for the specific heat that we have found in the statistical treatment (Equation 5.9). This expression is valid for the condensed part. For the thermal atoms, the specific heat does not depend of either the pressure parameter or the volume parameter for high temperatures.

After showing that, for an ideal gas, the global variables provide the same result as the conventional approach, we will take advantage that in the global variables it is easy to treat interacting systems, to study the effect of the interaction in the specific heat.

5.2 Effects of interaction on the specific heat

When the interaction is taken into account, the Hamiltonian for the system has one more term and the pressure parameter becomes proportional to the integration of the density. As already discussed, the density of an *interacting* Bose gas is well established to obey a Thomas-Fermi distribution for the condensed part, and a Gaussian distribution for the thermal part. For this comparison we are considering just 1D, then the densities are given by

$$n_{BEC}(x,y,z) = \frac{15N_{BEC}}{8\pi R^3} \max\left[1 - \left(\frac{r}{R}\right)^2, 0\right] \tag{5.24}$$

and

$$n_{th}(x,y,z) = \frac{N_{th}}{(2\pi)^{3/2}\sigma^3} \exp\left[-\frac{1}{2}\left(\frac{r}{\sigma}\right)^2\right]. \tag{5.25}$$

Using these equations above, we evaluate Equation 3.15, obtaining the final equations for the two components of the pressure parameter

$$\Pi_{BEC} = \frac{mN_{BEC}}{21\mathcal{V}} 3\left(\omega^2 R^2\right) \tag{5.26}$$

$$\Pi_{th} = \frac{mN_{th}}{\mathcal{V}}\left(\omega^2\sigma^2\right). \tag{5.27}$$

Now that the equations for the pressure parameter were obtained, we just need to derive it with respect to temperature to obtain the specific heat. Here the pressure parameter has two components, and the specific heat will be

$$C_{\mathcal{V}} = \begin{cases} 3\mathcal{V}\left(\frac{\partial(\Pi_{BEC}+\Pi_{th})}{\partial T}\right)_{N,\mathcal{V}}, & \text{for } T < T_C \\ 3\mathcal{V}\left(\frac{\partial \Pi_{th}}{\partial T}\right)_{N,\mathcal{V}}, & \text{for } T > T_C \end{cases} \tag{5.28}$$

This expression is valid for an interacting system, and since we have obtained the specific heat also for an ideal gas, we can compare both expressions to see the effect of the interaction. In Figure 8 we show the specific heat evaluated for both the interacting and ideal gas.

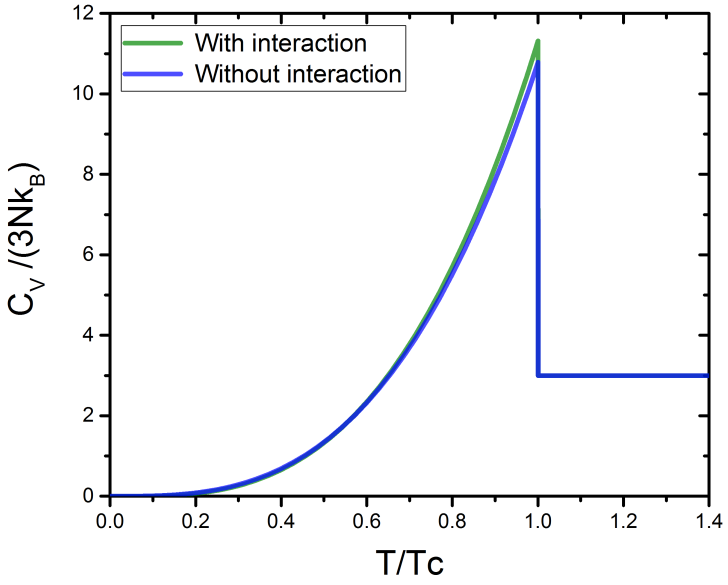

Figure 8 – Specific heat as a function of temperature. In blue we show the specific heat evaluated from an ideal gas. In red we show the effect of interaction in the specific heat. The interactions were taken into account in the pressure parameter.
Source: By the author.

In this comparison we see that the interaction almost does not change the behavior of the specific heat. For very low temperatures the curves are very close to each other, and they start to separate when the temperature is close to the transition.

This is expected in the temperature scale where the condensations takes place. For very low temperatures, the interaction potential between atoms is governed by the s-wave scattering. In this model of scattering, the interacting potential is given by $g = 4\pi\hbar^2 a/m$, with a the s-wave scattering length, that does not depend on temperature.

Then, we can conclude that the small deviation that we have found on the specific heat when the interaction were considered, may be associated with small variation at the energy level of the system. Also, we may associate it with small corrections at the interaction potential with the temperature, since the deviation only appears for higher temperatures.

We know that this comparison is not very accurate because we assumed the bi-modal model to simulate the density of the cloud. In this model, the Thomas-Fermi approximation is used for the condensed part and it results in a parabolic shape for the density. For thermal atoms it is assumed that the density obeys a Gaussian distribution. What we emphasize in this model is that the interaction between BEC and thermal atoms is not taken into account, and it could lead to a higher difference in the specific heat.

There are other methods that consider the interaction between BEC and thermal atoms, but to obtain the density profile we need to make numerical integration, since they do not provides analytic solutions for the density.

Numerical simulations (79) shows that there is no big differences in the density profile when interaction between thermal and condensed atoms is considered. However, the density is not what determine the characteristic of the specific heat, but is the energy. We can expect that if these interactions were considered, the specific heat would be different from what we have obtained.

For a simple comparison, we think that our results present good accordance what is expected for the specific heat, and a more accurate comparison would need a more

elaborated theory for the global variables.

5.3 Compressibility and equation of state for an interacting gas: LDA versus global variables

In the last section we have shown that for a non interacting system the global variables provide the same results that the conventional variables. We also have done a simple study showing the effect of the interaction in the specific heat.

Here we make another comparison, comparing the GV and the local-density approximation, that is a widely used method to study properties of the trapped gases.

We start developing the LDA to find expressions that we can compare with the GV. Immediately after we will write the same expressions using the global approach and then we will make the comparison between these approaches.

All data in this comparison were obtained using this parameters: $N = 1 \times 10^5$ atoms, $\omega = 2\pi \times 30$ Hz and $T = 60\,\mathrm{nK}$, except when one of them is variable.

5.3.1 Compressibility and equation of state in the LDA

Local density approximation consists in considering that the cloud is composed by discrete portions where the density is uniform, and we can define local properties for each position. Since the density of the cloud reflects the trap potential, we can make a change of variables, writing the density as a function of the potential instead of the position.

This procedure was used in reference (35) to study thermodynamics in a Fermi gas. For that system, they measured the density as a function of the local potential and they

could observe the signatures of the phase transition after evaluating a few thermodynamic variables. Here, we will evaluate some of these variables using the global approach to see if they are equivalent.

A very useful way to characterize a system is by means of the equation of state (EoS). The most known EoS, the ideal gas law, is clearly not useful to describe a trapped Bose gas at low temperatures. For this system, we can find other thermodynamic variables that can express its behavior in a more appropriated way. We are going to write an equation of state which is valid and appropriate for this system. We start with the achievement of these state variables which will allow us to find an equation of state.

Thanks to the Gibbs-Duhem relation (51) $SdT - VdP + Nd\mu = 0$, at a given temperature we find a relation between the variation of the pressure and the chemical potential

$$dP = \frac{N}{V} d\mu = n d\mu, \tag{5.29}$$

which can be rearranged to obtain

$$n = \left(\frac{dP}{d\mu}\right)_T. \tag{5.30}$$

In harmonic trapping potentials the density is not uniform, and we see that the last equation is one equation of state for this system (35) because it relates variations of two functions of state, the pressure and the chemical potential, in each position. However, we will see soon that the chemical potential is not a good variable to write the EoS.

For a more complete notation we need to write the dependence with the position

$$n(r) = \frac{dP(r)}{d\mu(r)}. \tag{5.31}$$

In a Bose gas, it is expected that some variables present a discontinuity at the transition for the condensation. The isothermal compressibility and the specific heat are clear variables which present an abrupt change of behavior at the transition.

We start with the compressibility which is defined to be proportional to the variation of the volume for a change in pressure, or

$$\kappa = -\frac{1}{V}\left(\frac{\partial V}{\partial P}\right)_T. \tag{5.32}$$

The volume is not so much useful in LDA, because thermodynamic is written to be local. For this reason, instead of the volume we write the density $n = N/V$. We have $dV = -\frac{N}{n^2}dV$ and Equation 5.32 becomes

$$\kappa = \frac{1}{n(r)}\left(\frac{\partial n(r)}{\partial P}\right)_T. \tag{5.33}$$

However, the chemical potential can not be directly measured, but it is related with the local potential, $d\mu(r) = -dU(r)$ *. The potential can be found because the density profile of the cloud provides information from it, then measurements of the local density reveal the local potential.

Using this information we can write the compressibility as

$$\kappa = -\frac{1}{n(r)^2}\left(\frac{\partial n(r)}{\partial U(r)}\right)_T. \tag{5.34}$$

Also, it is possible to write the local pressure by using Equation 5.31. Solving for the pressure and integrating we have

$$P(U) = \int_{U(r)}^{\infty} n(U')dU', \tag{5.35}$$

where we have used the relation between the chemical potential and the trapping potential.

For the analysis we will consider a harmonic trapping potential with the form

$$U(r) = \frac{1}{2}m\omega^2 r^2. \tag{5.36}$$

Now, we will make a change of variables to write the properties of the gas as a function of the potential instead of the position. To do it, we need to isolate r in the last equation to obtain

$$r = \sqrt{\frac{2U}{m\omega^2}}. \tag{5.37}$$

In order to show how is the density written as a function of this potential, we plot it in Figure 9. In (a) the density is shown as a function of the position from the center of the cloud, and in (b) it is plotted as a function of the harmonic potential. In (a) one can easily see the change from thermal to condensate at about $10\,\mu$m, in (b) it occurs at around $0.02\,\mu$K.

* This relation is obtained by the effective potential $\mu(r) = \mu_0 - U(r)$

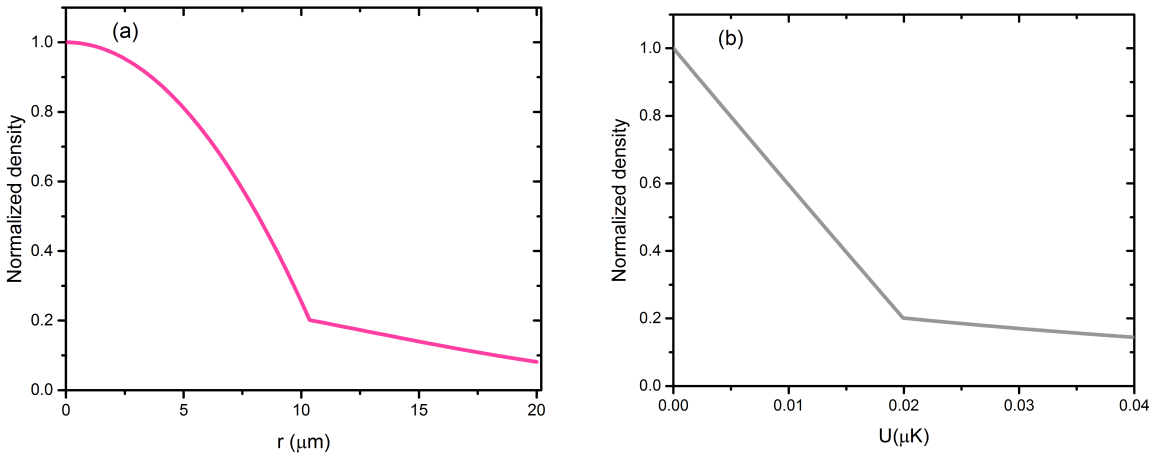

Figure 9 – Normalized density of the cloud as a function of the (a) position from the center of the cloud and (b) the potential.
Source: By the author.

Figure 10 shows the compressibility of Equation 5.34 as a function of the potential. Since our objective is to compare the two approaches, and the global variables do not have the same units of the usual pressure and volume, we normalized the compressibility by its maximum value. We see in this figure that the compressibility presents a peak at the transition between the thermal and the condensed components.

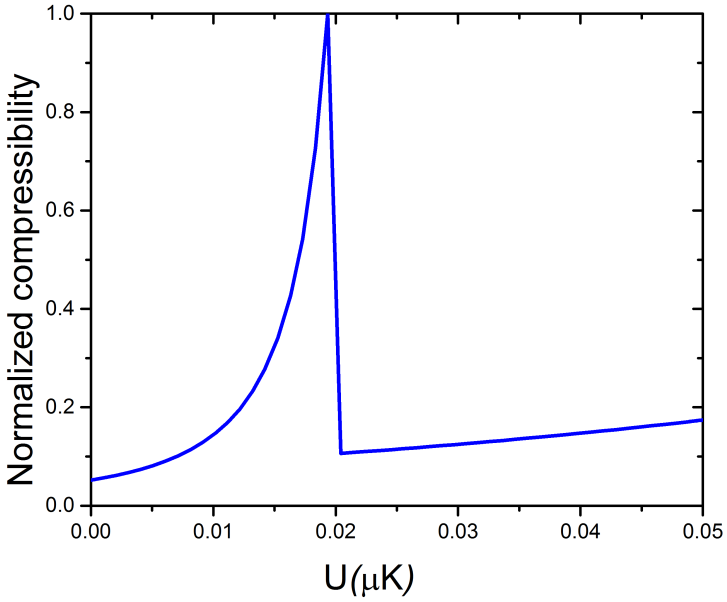

Figure 10 – Normalized compressibility as a function of the potential. The compressibility is normalized by its maximum value at the transition from the thermal to the condensed component.
Source: By the author.

Until now we have written the compressibility and the pressure as a function of

the position, i.e, as a function of the potential. This means that for each position we can evaluate pressure and compressibility. If we write the compressibility as a function of the pressure, one obtains an EoS for this system. The graph of this EoS is presented in Figure 11.

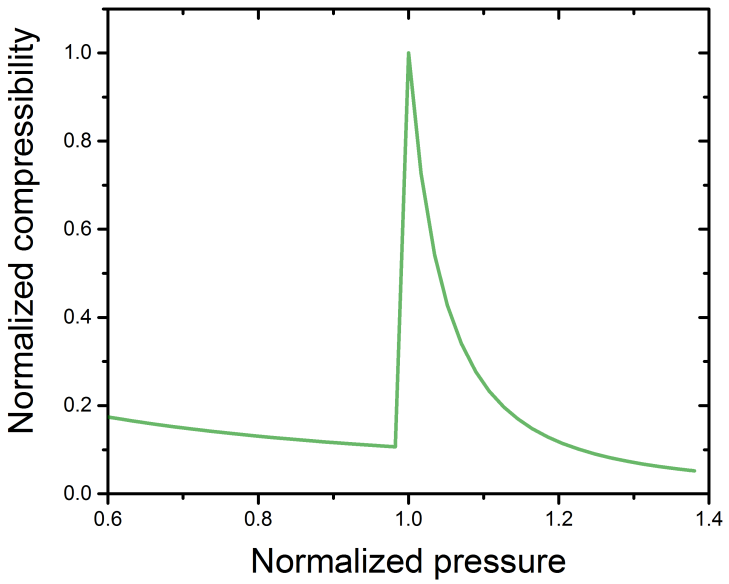

Figure 11 – Normalized compressibility as a function of the normalized pressure. The compressibility was normalized by its maximum value and the pressure was normalized with the value where the compressibility is maximum.
Source: By the author.

In what follows we are going to obtain the equivalent quantities using the global approaches and then compare both.

5.3.2 Global compressibility and EoS

In this section we will write the compressibility and the global EoS to test it against the local density approximation. Global variables do not use the assumption that the thermodynamic variables are dependent on the position. Instead, we have only global parameters which may be enough to describe the system.

The global compressibility is *defined* in reference (42) as

$$\kappa_G = -\frac{1}{\mathcal{V}}\left(\frac{\partial \mathcal{V}}{\partial \Pi}\right)_T , \tag{5.38}$$

where $\mathcal{V}$ is the volume parameter and Π is the pressure parameter. We see great similarity with the usual definition of the compressibility (See Equation 5.32), but for the GV we have other parameters.

Since these parameters are defined globally, we do not need to make any replacement to write it locally. In Figure 12 we show the isothermal compressibility as a function of the global volume parameter, where one can see that it presents a similar behavior to the LDA compressibility at the transition.

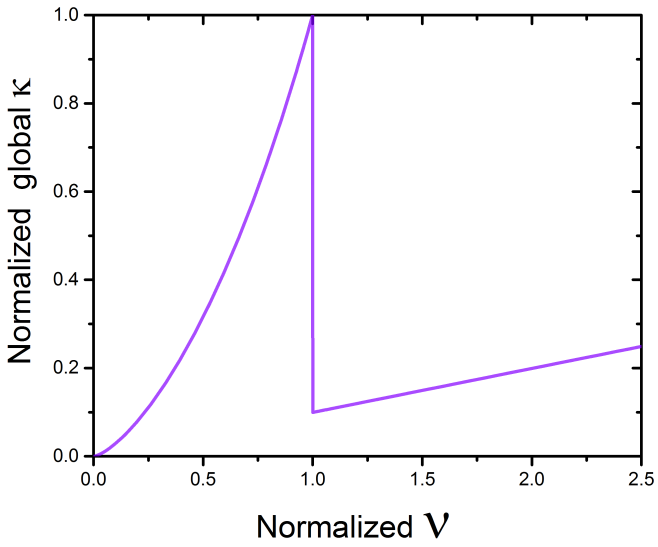

Figure 12 – Normalized global compressibility as a function of the normalized volume parameter. The global compressibility was normalized by its maximum value and the volume parameter was normalized with the value where the compressibility is maximum.
Source: By the author.

With the compressibility we also can find an EoS in the global approach. Similarly as it was done for the LDA, we show in Figure 13 the global compressibility versus the global pressure.

In this graph we see great similarity with the EoS obtained by using the LDA. In what follows, we will make a more clear comparison of these two approaches, LDA and GV, for the quantities that where defined independently for each method.

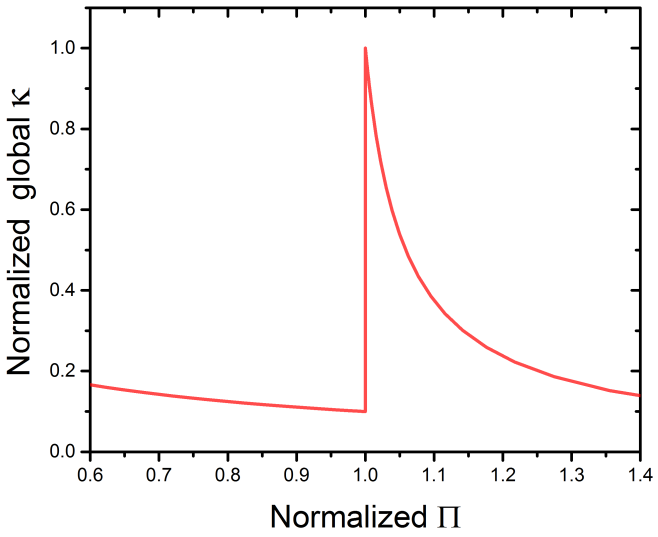

Figure 13 – Global equation of state (κ vs Π). The global compressibility was normalized by its maximum value and the global pressure parameter was normalized with the value where the compressibility is maximum.
Source: By the author.

5.3.3 Comparison

First we have evaluated the compressibility using both approach, and it is possible to see in Figures 10 and 12 that the behaviour is similar, but not identical. It happens because in the local approach we plotted the compressibility as a function of the potential, while in the global approach we have plotted it as a function of the volume parameter.

We see that although both are not identical, the isothermal compressibility has the same behaviour independently of the approach used to obtain it. The main differences are in the condensed part, where is clear that both approaches do not coincide at the origin.

Since the global variables do not have the same meaning of the usual definitions of pressure and volume, we can not expect that the global compressibility gives the same numerical values than the usual definition of the compressibility.

Now we will compare how is the EoS in both methods. We have previously found the EoS independently for both, LDA and GV, and we could observe that both present a similar behavior. To make it more clear we present both together in Figure 14. Now it is more evident that the equation of state presented in this picture is independent of the

approach used to obtain it. Small differences are more visible in the thermal part, but for the condensed they are almost equal. The peak is evident in both methods and the difference in the width is insignificant for the evidence of the transition. Moreover, the imprecision in measurements may lead to a broadening in the peak. (35)

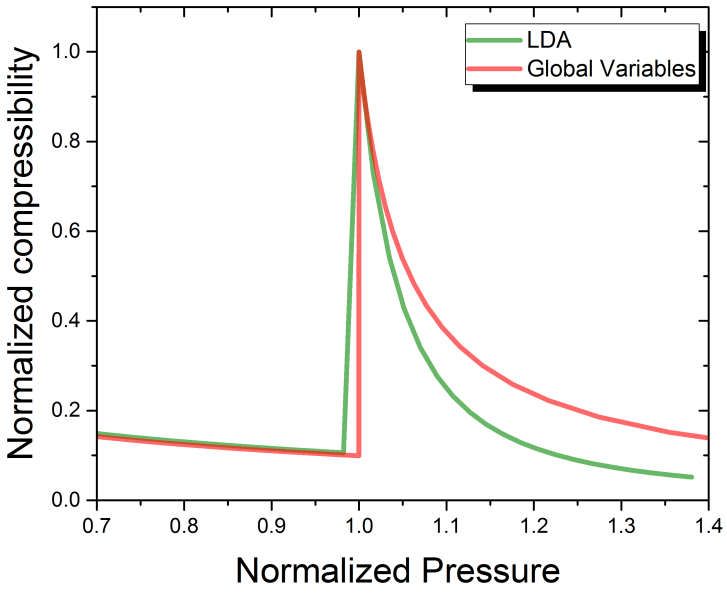

Figure 14 – Comparison between the EoS evaluated in both approaches. The normalization was done following the method presented in previous figures
Source: By the author.

In conclusion, we could show that the global variables can be an alternative to study thermodynamics in trapped gases. With this comparison we can not claim that one method is better than the other, because the comparison showed that they are equivalent.

We can say that both methods are good enough to show the singularities at the phase transition, such as shown for the specific heat and the isothermal compressibility. Both can present advantages dependent on the purpose. As discussed in reference (35), the LDA presents advantages over other methods because we can extract thermodynamic properties without making any fitting, since all quantities are obtained by measurements of the density.

However, the LDA is not an efficient tool to study thermodynamics in a cloud with many vortices. In a region with a vortex, the density can vary abruptly, and we will lose important information about the system if we are not able to map the density in an appropriate way. On the other hand, although been dependent on fittings, the global

approach is not sensible to local perturbation or singularities, and we can eventually study how vortices and perturbations modify the thermodynamic properties of the BEC.

6 Sound velocity determination using global termodynamic variables

As we have shown in Chapter 3, thermodynamic global variables can be applied in studing properties of a trapped Bose gas. One advantage is that the pressure and the volume parameter are easily obtained from standard methods of analysis. The first measurement using this approach was the phase diagram for ^{87}Rb, where using the variation of the pressure parameter as a function of the temperature, for different number of atoms, one obtains the critical temperature for the transition. (40) Then, the heat capacity at constant volume parameter was found to be proportional to the variation of the pressure parameter as a function of temperature. (41) Exploring the variation of the volume and the pressure parameter, was also possible to measure the isothermal compressibility (42) in terms of the global variables.

Here, we use the global variables to measure the sound velocity in a wide range of temperature, above and below the critical temperature and we compare with the expected value of the sound velocity for zero temperature, known as Bogoliubov sound velocity. We found the expected theoretical value for the sound velocity at zero temperature and we identify the contribution of each component, normal and superfluid, for this velocity.

6.1 Background

The equation for the sound velocity in Bose-Einstein condensates at *zero temperature* was first derived by Lee and Yang (80) based on the Bogoliubov theory for the

superfluidity, and it is frequently refereed as the Bogoliubov speed of sound, given by

$$c_B^2 = \frac{n(r)U}{m} \tag{6.1}$$

where $U = 4\pi\hbar^2 a/m$ is the interaction parameter for bosons with mass m and scattering length a.

In 1997 (81), it was published the first measurement for wave propagation in BEC. In that experiment, they used a laser beam detuned far off-resonance to induce density perturbations in the BEC. The laser was focused into the center of the trap and after the condensed had formed it was turned on, expelling the atoms from the center. Also, the condensate was produced in the presence of this laser beam and to generate the perturbation the laser was switched of.

The propagation of the perturbation travel with the speed of the sound, and multiples images from the same cloud allowed to measure this velocity. The first measurement did not complete agree with the equation for the sound velocity given by equation 6.1. Since the density of the cloud is not uniform for harmonic traps, the equation should be written in terms of the average density $\overline{n} = n_0/2$, where n_0 is the density at the center of the cloud. Using this consideration they found (82)

$$c_B^2 = \frac{n_0 U}{2m}, \tag{6.2}$$

and the results better fitted with the theory. These results also were confirmed theoretically by Zaremba (83) and Kavoulakis (84) by simulating a wave propagation induced in the BEC, the same way as it was done in the experiment.

Considering the Bose-Einstein condensation at *zero temperatures* does not treat the most general condition. Bose-Einstein condensation takes place at a critical temperature (which is not zero), and below this value the fluid has two components, normal and condensed. The sound velocity in the condensate may be affected by the presence of thermal atoms.

The sound velocity in this condition can be obtained by using the theory developed by Landau (85) for two-fluid systems. This theory was orinally developed by Landau to

study the superfluidity observed in ^{4}He in 1938 (5–6), but it is valid for any Bose fluid of two components.

Details about the Landau theory for the two fluids, and the derivation of the equations to evaluate the sound speed are found in references. (54, 86–87) Here we will focus only on the main results.

The basis of the Landau theory starts by writing the equation for the density of the fluid that obeys the continuity equation

$$\frac{\partial \rho}{\partial t} + \nabla \cdot (m\mathbf{j}) = 0 \tag{6.3}$$

and the linearized Euler equation

$$m\frac{\partial \mathbf{j}}{\partial t} = -\nabla p \tag{6.4}$$

where $\mathbf{j}$ is the current density and p is the pressure of the fluid. Here we have introduced the mass density ρ, that is related to the number density ($n = N/V$) by $\rho = nm$. According to the Landau theory, the superfluid part can be separated from the normal component, so, we can write the fluid density as the sum $\rho = \rho_s + \rho_n$ of a superfluid and a normal component moving with independent velocities $\mathbf{v}_s$ and $\mathbf{v}_n$. Then, the mass current is given by

$$m\mathbf{j} = \rho_s \mathbf{v}_s + \rho_n \mathbf{v}_n. \tag{6.5}$$

Now we need to obtain an equation for the entropy. If there is no dissipation, we can consider that the entropy is conserved and its transport is governed by the velocity of the normal fluid $\mathbf{v}_n$. In this way, the entropy can be written in the form of a continuity equation

$$\frac{\partial s}{\partial t} + \nabla \cdot (s\mathbf{v}_n) = 0 \tag{6.6}$$

where s is the local entropy density (entropy per unit volume). It is assumed that the two component are in local equilibrium and obey the Gibbs-Duhem equation

$$\rho \mathrm{d}\mu = -ms\mathrm{d}T + \mathrm{d}p. \tag{6.7}$$

By taking the gradient of Equation 6.4 and then using Equation 6.3, we obtain

$$\frac{\partial^2 \rho}{\partial t^2} = \nabla^2 p, \tag{6.8}$$

which is a important relation between the temporal variation of the density with the spatial variation of the pressure.

Now, in order to find a similar expression for the entropy, we can write Equation 6.6 in terms of the entropy per unit mass $\tilde{s} = s/\rho$

$$\frac{\partial(\tilde{s}\rho)}{\partial t} + \nabla \cdot (\tilde{s}\rho \mathbf{v}_n) = 0. \tag{6.9}$$

The second term of the left side of this equation can be replaced using Equation 6.3 to obtain

$$\frac{\partial \tilde{s}}{\partial t} - \frac{\tilde{s}}{\rho}\nabla \cdot (m\mathbf{j}) + \frac{\nabla \cdot (\tilde{s}\rho \mathbf{v}_n)}{\rho} = 0. \tag{6.10}$$

Now, using Equation 6.5 and rearranging the terms we have

$$\frac{\partial \tilde{s}}{\partial t} + \frac{\tilde{s}\rho_s}{\rho}\nabla \cdot (\mathbf{v}_n - \mathbf{v}_s) = 0, \tag{6.11}$$

which can be written as

$$\frac{\partial^2 \tilde{s}}{\partial t^2} = \frac{\tilde{s}^2\rho_s}{\rho_n}\nabla^2 T. \tag{6.12}$$

To obtain the last equation we have used Equations 6.6 and 6.7.

Since $\rho \equiv \rho(p, T)$ and $\tilde{s} \equiv \tilde{s}(p, T)$ we can expand its derivative

$$\delta\rho = \frac{\partial \rho}{\partial p}\delta p + \frac{\partial \rho}{\partial T}\delta T \tag{6.13}$$

$$\delta\tilde{s} = \frac{\partial \tilde{s}}{\partial p}\delta p + \frac{\partial \tilde{s}}{\partial T}\delta T \tag{6.14}$$

and we identify that equations 6.8 and 6.12 are coupled equations for pressure and temperature.

Solving the coupled equations by looking for plane wave solutions like $e^{i\omega(t-x/c)}$ and using a few thermodynamic relations we find that the sound velocity is is the solution of

$$c^4 - \left[\left(\frac{\partial p}{\partial \rho}\right)_{\tilde{s}} + \frac{\rho_s k_B T \tilde{s}^2}{\rho_n \tilde{c}_V}\right] c^2 + \frac{\rho_s k_B T \tilde{s}^2}{\rho_n \tilde{c}_V}\left(\frac{\partial p}{\partial \rho}\right)_T = 0, \tag{6.15}$$

where $\tilde{c_V} = T\left(\frac{\partial \tilde{s}}{\partial T}\right)_\rho$ is the specific heat at constant volume. This equation shows that if the supefluid density is not zero there are two solutions for the sound velocity.

The existence of two velocities is due to the presence of two fluids, where the first/second sound involves *in-phase*/*out-of-phase* motion of the superfluid and normal

fluid components. If $\rho_s = 0$ there is just a solution, and this is the usual sound velocity for a normal gas. If $\rho_n = 0$ it can be shown (57) that the solution for this equation recovers the Bogoliubov sound, given by Equation 6.2.

The meaning of the two velocities can be understood if we consider what happens when a fluid is perturbed. The sound velocity for a normal fluid is defined as the variation of the pressure as a function of the density. It means that when a density perturbation is induced in a fluid, this perturbation will propagate with a velocity that is referred as the sound velocity.

However, when a BEC below the critical temperature is perturbed, the motion between the two components can also induce a temperature wave, which will propagate with a velocity different from the density wave. These two velocities are called first (density wave) and second sound (temperature wave).

Density perturbation can be generate by an abrupt variation in the BEC density, as it was done in the first measurement. On the other hand, a temperature wave is only generated if the external perturbation induce the out-of-phase motion between the two fluids.

Since in diluted gases the two components are weakly coupled, the out-of-phase motion is very difficult to be induced, and in general, most of external perturbation will produce an oscillation of the BEC with the non condensed atoms staying at rest. For a strong interacting system, as a Fermi gas, the two fluids are coupled by interactions and the second sound velocity can be measured. (88)

The coupling between two fluids leads to Equation 6.15 which is not easily solved. This equation depends on many thermodynamic variables that not always have simple expressions. We can find exact solution for the sound velocities in the regimes of very low and very high temperatures. For very low temperatures, where $k_B T \ll \mu$, the first sound velocity is given by

$$c_1^2 = \left(\frac{\partial p}{\partial \rho}\right)_T \tag{6.16}$$

and the second sound velocity is given by $c_2^2 = \frac{1}{3}c_1^2$. (57, 87) Of course, at very low

temperature it is possible to show that this expression for the first sound approaches the zero-temperature Bogoliubov value given by Equation 6.1.

Knowing the dependence of the superfluid density with the temperature,

$$\rho_s = \rho \left[1 - \left(\frac{T}{T_c} \right)^3 \right], \tag{6.17}$$

and using some thermodynamic relations, one can show that at higher temperatures, $k_B T \gg \mu$, the *predominant* part of the first sound is given by

$$c_1^2 = \frac{5}{3} \frac{g_{5/2}}{g_{3/2}} \frac{k_B T}{m}, \tag{6.18}$$

and the second sound is

$$c_2^2 = \frac{\rho_s}{\rho} \left(\frac{\partial p}{\partial \rho} \right)_T, \tag{6.19}$$

where $g_{5/2} = 1.342$ and $g_{3/2} = 2.612$. To obtain Equation 6.18 reference (57) argue that in Equation 6.15 the derivative $\left(\frac{\partial p}{\partial \rho}\right)$ at constant *temperature* is small because the pressure in a ideal Bose gas does not depend on the volume, and then this equation for the first sound velocity is obtained only from the derivative $\left(\frac{\partial p}{\partial \rho}\right)$ at constant *entropy**.

It is possible to show that the equation for the second sound at higher temperatures results in the expression for the first sound at low temperatures. This feature is frequently refereed as the hybridization of the first and second sound. A good discussion and demonstration can be found in reference. (54)

6.2 Global sound velocity

Now, we are going to redefine the equation for the sound velocity writing it in terms of the global variables which were described in Chapter 3.

In Chapter 3 we showed that $\Omega = -PV = -\Pi\mathcal{V}$. It means that when we have expressions containing the *conventional* pressure and volume, we can study the same

* We will show in our results that we measure the term whose derivative is done at constant *temperature*, which is expected to be smaller.

properties by using the equivalent pressure and volume *parameters*, as it was done for the equation of state (37) for the heat capacity (41) and for the isothermal compressibility (42). The first sound velocity is given by

$$c_1^2 = \frac{\partial p}{\partial \rho}$$

and the density is $\rho = \frac{mN}{V}$, where N is the total number of atoms each with mass m confined in a volume V. Replacing the density we obtain that

$$c_1^2 = \frac{1}{m}\frac{\partial p}{\partial\left(\frac{N}{V}\right)} \tag{6.20}$$

which depends on the pressure and the volume. It means that we can obtain a similar equation in terms of the global pressure and volume.

Motivated by the last expression, we *define* the global sound as

$$c_{1g}^2 = \frac{\partial \Pi}{\partial \rho} \tag{6.21}$$

which, after to replace the density, results a similar expression for the sound velocity

$$c_{1g}^2 = \frac{1}{m}\frac{\partial \Pi}{\partial\left(\frac{N}{\mathcal{V}}\right)}. \tag{6.22}$$

The volume parameter $\mathcal{V}$ only depends on the trapping frequencies, what means that it is always constant since the trap parameters are not modified, which leads to

$$c_{1g}^2 = \frac{\mathcal{V}}{m}\frac{\partial \Pi}{\partial N}. \tag{6.23}$$

that is the global sound velocity for the cloud. We can observe in this equation that the sound velocity can be evaluated by computing the variation of Π with N. Since we can evaluate this variation for a constant temperature, we will determine the sound velocity as a function of temperature.

We need to draw attention to the units of the sound speed. Although either Π and $\mathcal{V}$ separately do not have units of the usual pressure and volume, we can check which the global sound velocity is really expressed in velocity units.

As can be seen by Equation 3.20, the pressure parameter is proportional to the hydrostatic pressure. It means that the global sound velocity is related to the local sound

velocity, and is possible to find the equation which relate both. The direct relation that the global sound velocity has with the local sound velocity is still being investigated.

What we can observe is that since the local pressure varies for a cloud trapped in a harmonic potential, the sound velocity will be depend on the position. In contrast, each cloud has only one pressure parameter and in consequence, it has only one global sound. Then, the main difference between both is that the usual sound velocity is locally defined, while the global sound is defined globally.

Now we are going to describe the procedures to measure the sound velocity in the cloud.

6.3 Experimental sequence

In equation 6.23 we see that the global sound velocity is determined by the variation of the pressure parameter with the number of atoms. For this measurement, the number of atoms and its temperature need to be changed in order to obtain a wide range of data to determine the sound velocity as a function of temperature. In the experiment, the final number of atoms can be controlled by the initial number of atoms loaded in the magnetic trap and/or by the evaporative cooling process that is performed to cool down the sample.

Figure 15 summarizes the procedure to evaluate the sound velocity. Changing the number of atoms and the temperature, we run the experiment continuously to obtain a large set of data. We analyze the data with the appropriated fitting function as described in Section 4.7, which provides the temperature, number of atoms and dimensions, that are the most relevant information for evaluating the sound velocity.

All measurements are performed in time-of-flight, and to obtain the *in situ* radii we use the Castin-Dum regression (89) that provides the dimensions of the cloud in trapping.

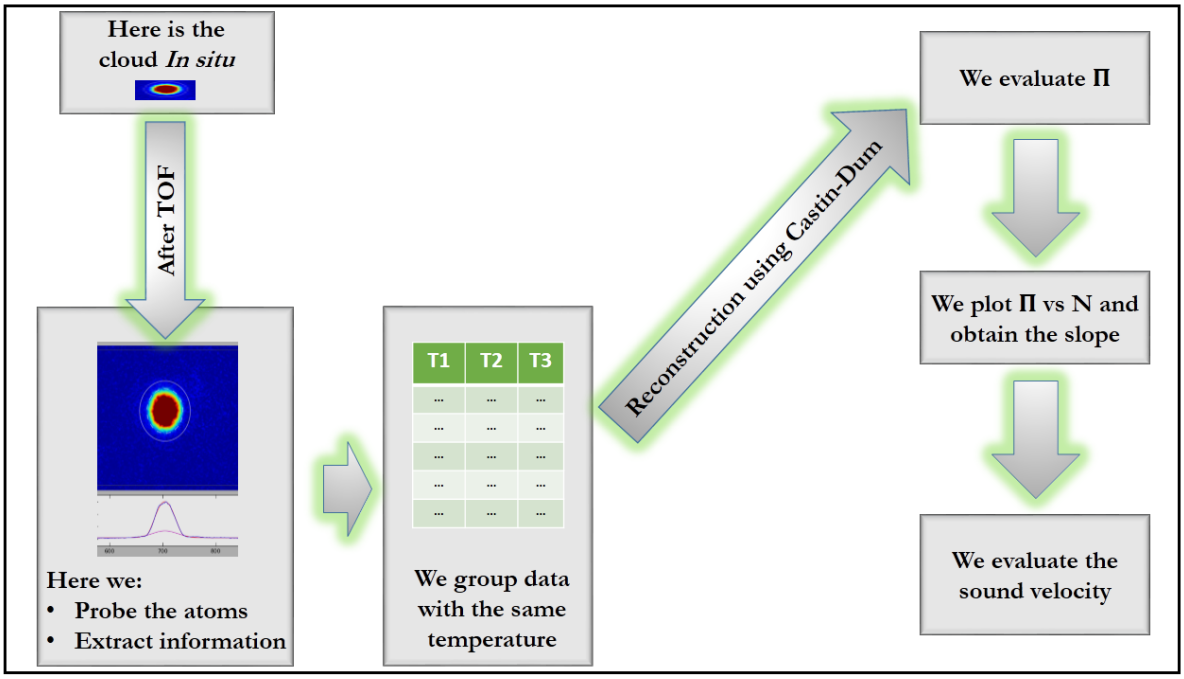

Figure 15 – Sequence used to evaluate the sound velocity. The measurements are performed in TOF to avoid saturation. We use fitting functions to extract all information of the cloud. Then, we group images in the same range of temperatures. With this data we plot the pressure parameter versus the total number of atoms, from where we extract the slope. With the slope of these graphs we can evaluate the sound velocity as discussed in the text.

Source: By the author.

The Castin-Dum regression is well established for determining the dimensions of the cloud as a function of the TOF, and our measurement are in good agreement with the method.

For TOF lower than 15 ms the cloud has a high density, and can saturate the image, what would lead to unreliable data. For this reason, we choose to take all measurements in 23 ms of time-of-flight.

With all data we use Equations 3.18 and 3.19 to evaluate the pressure parameter for the condensed and thermal part respectively, and since the sound velocity depends on the temperature, we group together all data in the same temperature range within ± 5 nK.

For each temperature we plot the pressure parameter versus the number of atoms as shown in Figure 16 that presents typical data for three different temperatures. We observed that in these temperatures the variation of Π is linear with N. In fact, we found small deviation from the linearity **only for very low temperatures** and also for **small**

number of atoms. Since our measurements were done changing the number of atoms in a large scale, we have the majority of data obeying the linear behavior of Π vs N, and just a few points with number of atoms in the not linear region. Then, assuming that the behavior is linear, is expected that the confidence of our data for very low temperatures will be a slightly smaller than for higher temperatures.

From this information, we see that the quantity $\frac{\partial \Pi}{\partial N}$ in equation 6.23 is the slope of these curves, and multiplied by $\frac{\mathcal{V}}{m}$ results in the sound speed for a given temperature.

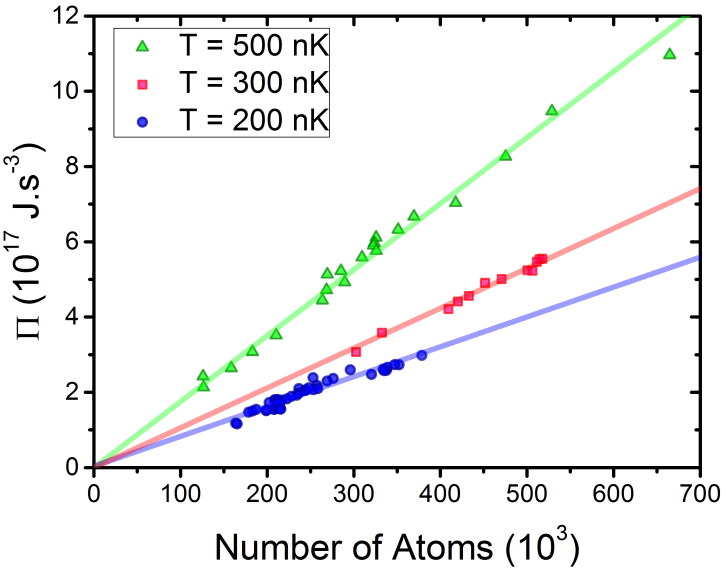

Figure 16 – Typical sets of data which are used to evaluate the sound velocity. Here the data are presented for three different temperatures to show the differences in the slope. The triangles are data for 500 nK, the squares are data for 300 nK and the circles are data for 200 nK. The lines for each temperature are linear fittings which we use to obtain the slope.

Source: By the author.

In our experiment the volume parameter is $\mathcal{V} = 5.4 \times 10^{-9}\,\mathrm{s}^3$ and the mass of ^{87}Rb atoms is $1.44 \times 10^{-25}\,\mathrm{kg}$. Just to give one example, the slope for $T = 200\,\mathrm{nK}$ is $7.66 \times 10^{-23}\,\mathrm{J \cdot s}^3$ and using Equation 6.23, it results in $c_{1g} = 1.69\,\mathrm{mm/s}$. Doing the same procedures, we can evaluate the sound velocity for all temperatures, whose results we will show in the next section.

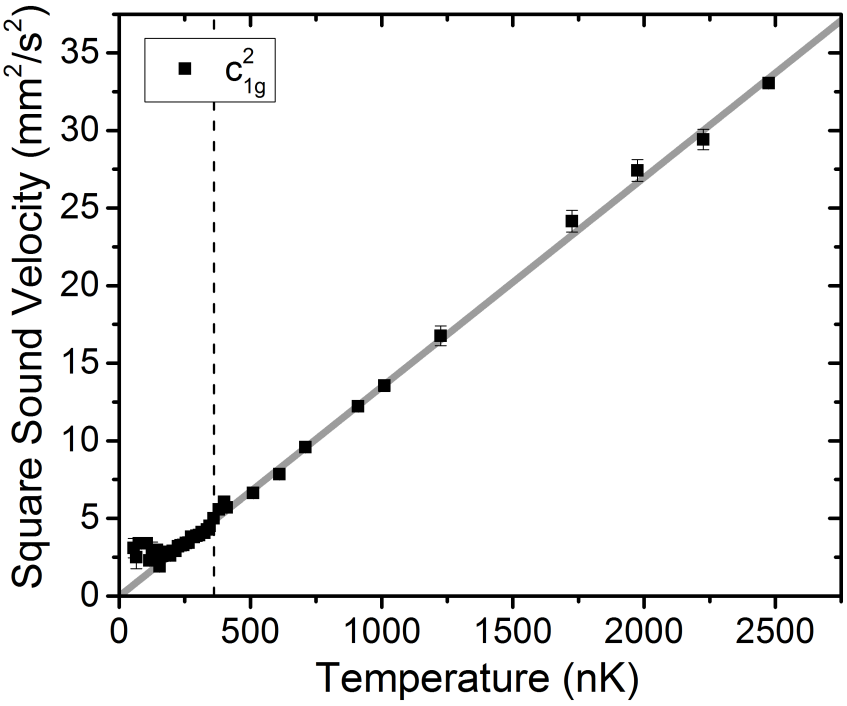

Figure 17 – Squared first sound velocity of a Bose-Einstein condensate as a function of temperature. The linear behavior is evident to the right of the vertical dashed line that represented the approximate critical temperature.
Source:By the author.

6.4 Results

We start showing in Figure 17 the global first sound velocity, c_{1g}^2, obtained from equation 6.23 for a wide range of temperatures. For the thermal part it is expected that the square sound velocity is linear with the temperature, and this is clear in Figure 17 above the vertical dashed line, which is approximate the critical temperature. The solid line is a linear fitting of the data above the dashed vertical line.

In Figure 18 we show the sound for a smaller range of temperature to emphasize the region which contain the superfluid. We show the value for the first sound at zero temperature, given by Equation 6.2, in the horizontal dashed line.. We see that the global sound velocity approaches the first sound when the temperature tends to zero. The vertical line is the approximate limit for where we observe just thermal atoms.

As discussed, Equation 6.18 is the predominant part of the first sound velocity and it was obtained after neglecting the term whose derivative is done at constant temperature.

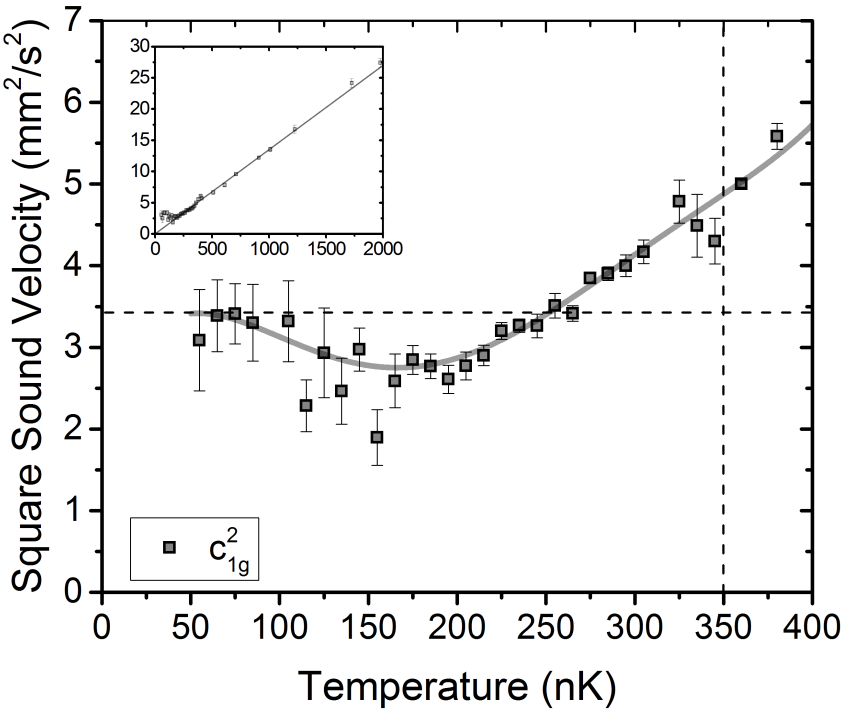

Figure 18 – Global first sound velocity as a function of temperature. Solid lines are guides for the eye following the points. Dashed horizontal line is the Bogoliubov sound speed, which is the theoretical sound velocity evaluated for zero temperature. Dashed vertical line is the approximate temperature for the critical temperature.
Source:By the author.

In our method, we do not know how to evaluate the entropy, and we can only determine the sound velocity at constant temperature, which is the less significant term of the equation. For this reason, we can not expect that our measurement for the sound velocity at higher temperatures gives the same result that when evaluated using equation 6.18. We evaluate the slope $(\Delta(c_1^2)/\Delta T)$ of this linear behavior with our method and also using Equation 6.18 and we found respectively $1.3 \times 10^{-2}\,\mathrm{mm^2 s^{-2} nK^{-1}}$ and $8.2 \times 10^{-2}\,\mathrm{mm^2 s^{-2} nK^{-1}}$.

Now we present one advantage of our method, which allows us to determine which fluid contributes more in each temperature. The pressure parameter of Equation 6.23 is given by the sum $\Pi = \Pi_{BEC} + \Pi_{th}$, and we can use this to separate the *first* sound as

$$c_{1g}^2 = c_{BEC-part}^2 + c_{th-part}^2 \tag{6.24}$$

with the components given by

$$c_{BEC-part}^2 = \frac{\mathcal{V}}{m}\frac{\partial \Pi_{BEC}}{\partial N} \tag{6.25}$$

and

$$c^2_{th-part} = \frac{\mathcal{V}}{m}\frac{\partial \Pi_{th}}{\partial N}. \tag{6.26}$$

Here we emphasize that the fluids *are not* independent, since in these equation the number of atoms involved in the total number. This separation represent the participation of each component for the first sound velocity.

With this separation, we present in Figure 19 the contribution of each component, BEC and Thermal, for the global first sound velocity. Here the solid lines are only guides for the eyes to show that there is a temperature where the most predominant part becomes the less one. Vertical and horizontal lines have the same meaning that in Figure 18.

We can see that around 150 nK there is an inversion of the influence for each component. Before this temperature, we see that the BEC is predominant and it inverts above this point, where the thermal part becomes more influential. This change in behavior is similar to the observed in reference (80, 90) and discussed in references (54, 57) and is commonly called hybridization between the first and second sound. Here is important to say that the hybridization of these references occurs for the first and second sound, and in our results the behavior occurs for the *contribution* of the BEC and thermal components in the *first* sound.

In addition, we also can analyze both fluids as if they were completely independent. If we evaluate

$$c^2_{BEC} = \frac{\mathcal{V}}{m}\left(\frac{\partial \Pi_{BEC}}{\partial N_{BEC}}\right)_T \tag{6.27}$$

and

$$c^2_{th} = \frac{\mathcal{V}}{m}\left(\frac{\partial \Pi_{th}}{\partial N_{th}}\right)_T, \tag{6.28}$$

in our understanding, we are evaluating the velocity of sound waves traveling in the condensate and in the thermal part independently as if they were only one fluid.

We know that

$$c^2_{1g} \neq c^2_{BEC} + c^2_{th}, \tag{6.29}$$

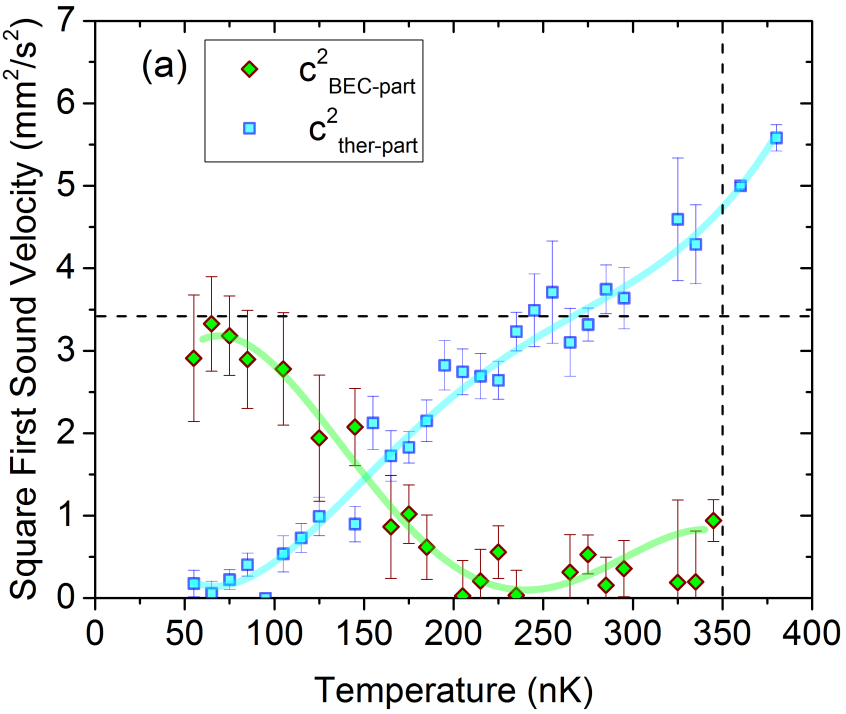

Figure 19 – Contribution of each component for the global first sound velocity. Blue squares are the contribution of the thermal part and green diamonds represent the contribution of the BEC. The solid lines are guides to the eye to show that around 150 nK the fluid with less contribution becomes the fluid which contributes more for the sound velocity. Horizontal and vertical lines have the same meaning that in Figure 18.
Source: By the author.

but treating separately the fluids can bring information of how the first sound in the BEC is affected by the presence of the thermal atoms, and we can compare it with a previous work.

Figure 20 shows the sound velocity for each component, evaluated from Equations 6.27 and 6.28.

In Figure 20 one can observe that the sound velocity in the thermal part is linear with temperature, as expected for a normal fluid and it tends to zero at zero temperature. For the condensate part, we can see that the sound speed oscillates around a value and does not present an abrupt change.

A similar behavior was observed in reference (91) when the sound velocity was studied as a function of the temperature. In that work, the authors induced density perturbations in the condensate and measured the velocity for these propagation. The manner as the sound propagation was induced is similar to the first measurement of the

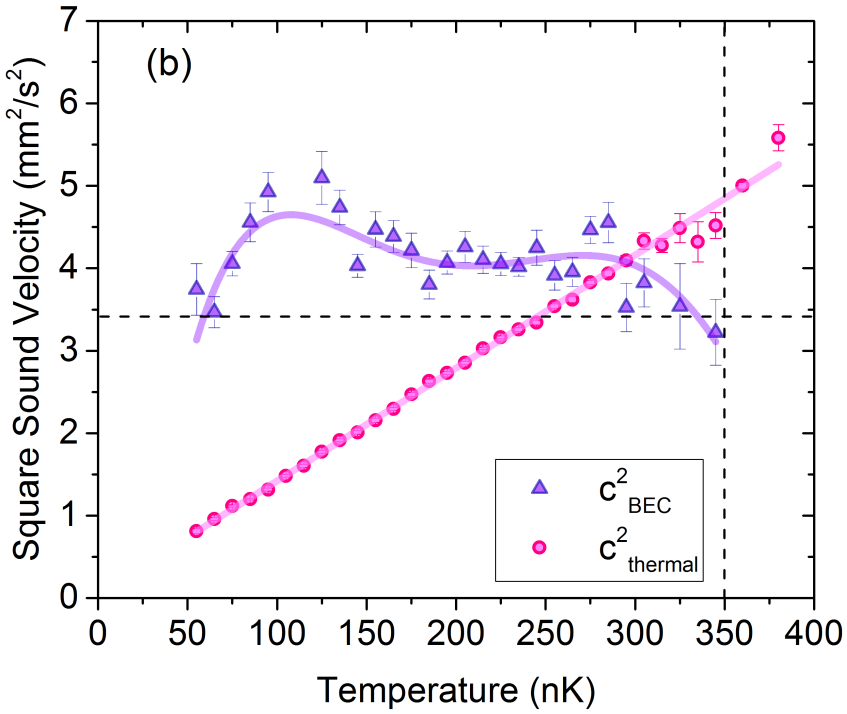

Figure 20 – Independent speed of sound in the BEC (violet up-triangles) and in the thermal part (magenta circles). To evaluate these velocity we treat each component separately as if thew were *totally independent* (see text). In this figure, the magenta solid line is a linear fitting for $c^2_{thermal}$ and the violet solid line is a guide for the eyes following the points. Dashed lines have the same meaning of the previous figures.
Source: By the author.

sound velocity of reference. (81)

They measure the propagation of the sound for many temperatures and mapped this dependence. The number of atom in the thermal part is totally dependent on the temperature, therefore variations in the temperature will lead to variation in the interaction between BEC and thermal atoms.

They found that the sound velocity in the BEC is almost constant with the temperature. We see in their measurements that the sound velocity oscillates around a normalized value but it almost does not change. For this reason, we can conclude that the thermal atoms do not modify the velocity of density perturbations in the BEC.

We may say that our measurement for c^2_{BEC}, presented in Figure 20, may be the same velocity which they measured, because for us the idea is almost the same. When we treated the fluids totally independent to evaluate c^2_{BEC}, we have evaluated the sound velocity in the BEC without to consider any thermal participation.

In our measurement for the c^2_{BEC} as a function of the temperature, we also found that the sound speed is almost constant around a value, and it leads to conclude that the thermal atoms almost do not affect the sound velocity in the BEC.

To summarizing this chapter, we have measured the sound velocity as a function of the temperature. We found expressions for the sound velocity in a new description using the global variables. We found good agreement with the theory of Bogoliubov for zero temperature, and also we found the same linear behavior expected for the sound propagation in thermal atoms.

Also, with this method we could treat the fluids totally independent, and it allowed us to determine how the velocity in the BEC is affected by the presence of thermal atoms. We found similar results of presented in the literature. Besides that, our measurement made it possible to determine the contribution of each component for the sound velocity, that, in our knowledge, it is the first time that it was possible.

7 Conclusions and prospects

We start this chapter summarizing the results obtained in this thesis, and then we give an overview about the prospects for research topics in our group and improvements in our experimental system.

7.1 Conclusions

This thesis was based on testing the validity of the global thermodynamic variables and in the measurement of the sound velocity using this approach.

In Chapter 6, we use the global thermodynamic variables to obtain equations for the sound propagation in trapped gases. Then, we could measure this sound velocity by studying the variation of the pressure parameter with the variation of the number of atoms.

We were able to make different analysis by separating the components of the pressure parameter and also separating the two fluids to treat them independently.

For the first global sound velocity, we found good agreement with theory for two regions where we could make a simple comparison, and we conclude that:

1. The dependence of the first sound with the temperature is linear for a normal gas;

2. The first sound approaches the Bogoliubov sound for very low temperatures.

We also could use our method to analyze which fluid contribute more in each temperature range. We could observe that for lower temperatures the BEC contribution is more expressive for the first sound velocity, and for higher temperatures it inverts, and the thermal atoms become more influential.

The last topic for the sound velocity was studying the fluids as they were completely independent. For this, we separated the two fluids and measured the first sound velocity in each component. For this measurement we observed that:

1. The sound propagation in the thermal atoms is linear with the temperature as expected for any normal fluid;

2. The sound propagation in the BEC is almost constant with the temperature and its value almost match the Bogoliubov value for zero temperature.

In a general way, the global variables have provided a simple way to measure the sound velocity in a Bose gas either in the BEC and thermal atoms. This method is more simple than produce density perturbation in the cloud, mainly in the thermal atoms, where the propagation of a density perturbation would be almost impossible to be observed.

In Chapter 5 we compare the global variables with other methods and we analyzed different properties of the BEC, such as the specific heat, the compressibility and one of the equations of state.

For the specific heat, we have studied the ideal and the interacting gas. We have shown that for an ideal gas the global variables yield exactly the same result that the statistical treatment found in standard thermodynamics.

Also, comparing the interacting and non interacting gas, we could see the specific heat is almost not affected by the interactions, and this can be expected since the interaction energy do not change in the typical scale of temperature that the Bose-Einstein condensation occurs. We could see a small deviation from the ideal gas that may be associated with the change in the energy levels, when the interaction is taken into account.

We also compare the global variables with the local-density approximation. Using these two methods we have evaluated the compressibility and the equation of state κ vs p.

For the compressibility we could reinforce that the volume parameter represent the effect of the potential over the atoms. Both approaches presented the typical peak on

the compressibility at the phase transition from thermal to condensate.

We plotted the compressibility versus the pressure using the local-density approximation, and we compared with the plot of the global compressibility versus the global pressure, and they present a great similarity.

With this comparison we conclude that both approaches are good enough to study thermodynamics. While LDA present the advantage of extract the density profile without making fittings, it is not applicable when there is great variations of density in the systems. On the other hand, the global variables are dependent on fittings, but they could be applied to the study of vortices and turbulence, and any perturbed system.

7.2 Prospects

Our group follows two main research areas: Thermodynamics using global variables and production of vortices and turbulence in superfluids.

In thermodynamics our group have published a few papers measuring the heat capacity, the compressibility, equation of state, among others. (36, 38–42) Also, there is a work in progress in measuring the thermal expansion coefficient.

In this topic, we intend to explore thermodynamics close to the phase transition, where we want to investigate the frontier between the BEC and the thermal atoms. We have interest in this region because there is not much investigation about it and we know that some properties are not well defined in this region.

Also these variables are important because they can be applied to study thermodynamics in perturbed BECs and also with vortices. Since the LDA can not be applied in systems with abrupt changes in density

On the other main area, our group has great interest in studying vortices and turbulence. The group is known by the first evidence of quantum turbulence (32–33) but

many other studies with vortices where published (27–31), as well as some investigating the evolution to and of a turbulent state. (43–44)

In order to investigate the vortex formation, and also the turbulence, in a more controlable way, we have implemented the technique of topological phase-imprinting. (46) In this method, vortices are produced by the inversion of the bias magnetic field and the charge of the vortex is proportional to the hyperfine state of the atoms.

In our experiment, since the experiment was built, the atoms were always produced in the $m_F = 2$ hyperfine state. For this state the charge of the vortex is $n = 4$.

The idea in producing this vortex is to study its decay. It is known that any multicharged vortex is unstable and it must to decay into unitary-charged vortex, but the details of the decay process has been constantly studied.

When we started to produce vortex using this mechanism, we soon observed an interference pattern that had not been reported in previous work where they used this method. Figure 21 shows what we see when the vortex is produced. These images were taken in a axis that is perpendicular to the line of the vortex.

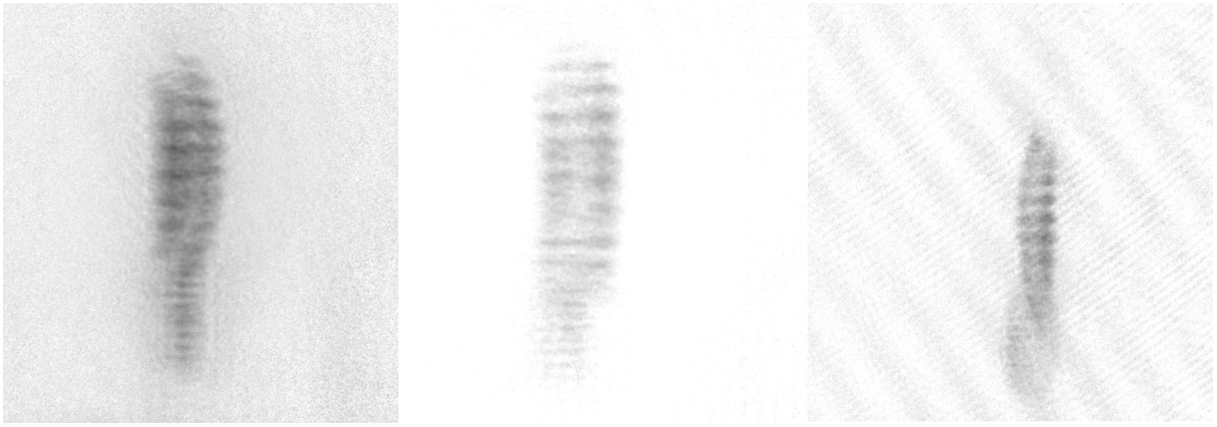

Figure 21 – Typical images of interference that appears when we make the bias inversion to produce vortex.

Source: By the author.

Although interference is evident when a BEC is separated and then recombined, in our method we do not separate the condensate. The way that the interference appears is not clear yet, and we are motivated to explore this.

This was one of the reasons why we started to produce condensates in the $F = 1$

state. When the bias is inverted, the condensate spend a short time in zero magnetic field, and it makes part of the atoms to be transferred to other states. One of these states is the $m_F = 1$, that also is magnetically trappable, and it appears as the smallest cloud in Figure 22. This two clouds are in different m_F states, but they were originated from the same cloud. These images were taken in an axis parallel to the vortex line.

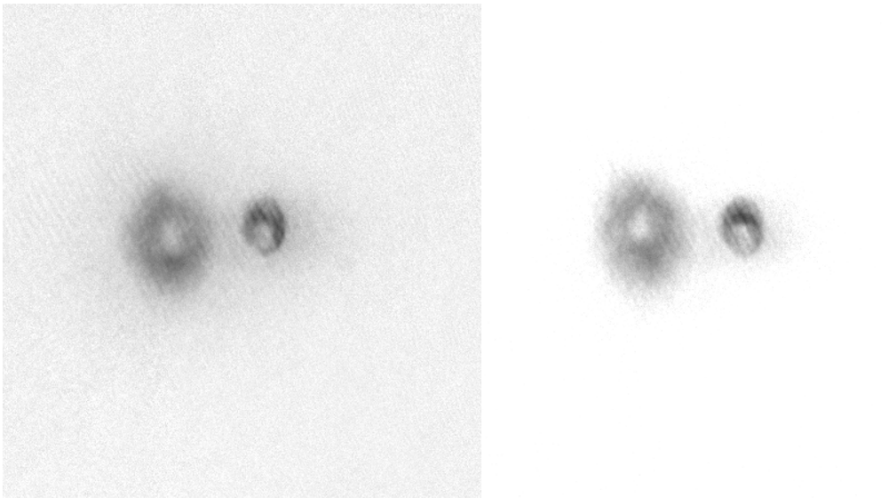

Figure 22 – Typical images of the vortex produced by the bias inversion. The clouds are in the two magnetically trapped states of the $F = 2$ state, $m_F = 2$ and $m_F = 1$.
Source: By the author.

The second cloud may be not desirable in some moments. For example, if we perturb the cloud to "maybe" accelerate the decay process, the two clouds can oscillate around each other and generate some inconvenient phenomenons, such as an overlapping, that may cover the effects.

On the other hand, the $F = 1$ state has only one sublevel Zeeman that is magnetically trappable. It means that when we invert the magnetic bias, the atoms that are transferred to another states will not return to the trap, and we will end with just a cloud in the trapping potential.

We are not able to produce vortex in the $F = 1$ state yet, but this is an important step in our goals. The production of vortex in the $F = 1$ state means that we will able to study vortex with different charges. Besides that, we will be able to investigate if the interference may provide information about the charge of the vortex.

At the moment, we are making the bias inversion in a way that do not produce

vortex, but that produces interference. We are going to make a further investigation to see if the interference give information about the vortex charge.

After this, we will spend more time trying to generate vortex in the $F = 1$ state to follow our goals in compare vortex of different charges.

Thinking about improvements, we want to implement other techniques of imaging and trapping in the next months. We are planning to implement a non destructive image system and also a pure optical trap or a hybrid trap.

The non destructive image will probably be the phase-contrast imaging (79), that presents many advantages over the absorption imaging. With this technique it is possible to take up to 100 images from the same cloud, allowing us to better study phenomena that evolves in time.

The optical trap also bring another prospects for the experiment. One of them is that the optical potential is easier to be controlled and the frequencies of it can be easily changed. More than this, with this optical trapping we also want to make experiments with turbulent clouds in a double well potential (92), an experiment that was never done to perturbed clouds.

With these implementations and the studies that are been proposed, we believe that the group will continue to produce a good work in this area.

References

1 BOSE, S. N. Plancks gesetz und lichtquantenhypothese. *Zeitschrift für Physik*, v. 26, n. 1, p. 178–181, 1924.

2 EINSTEIN, A. Quantentheorie de einatomigen idealen Gases-Zweite. *Sitzungsberichte der Preussischen Akademie der Wissenschaften*, v. 1, p. 3–14, 1925.

3 PENROSE, O.; ONSAGER, L. Bose-Einstein condensation and liquid Helium. *Physical Review*, v. 104, n. 3, p. 576–584, 1956.

4 LONDON, F. The λ-phenomenon of liquid Helium and the Bose-Einstein degeneracy. *Nature*, v. 141, p. 643–644, 1938.

5 KAPITZA, P. Viscosity of liquid Helium below the λ-Point. *Nature*, v. 141, n. 3558, p. 74, 1938.

6 ALLEN, J. F.; MISENER, A. D. Flow of liquid Helium II. *Nature*, v. 141, n. 3558, p. 75, 1938.

7 HECHT, C. E. The possible superfluid behaviour of hydrogen atom gases and liquids. *Physica*, v. 25, p. 1159–1161, 1959. doi: 10.1016/0031–8914(59)90035–7.

8 STWALLEY, W.; NOSANOW, L. Possible "new" quantum systems. *Physical Review Letters*, v. 36, n. 15, p. 910–913, 1976.

9 GREYTAK, T. et al. Bose-Einstein condensation in atomic hydrogen. *Physica B*, v. 280, n. 1-4, p. 20 – 26, 2000.

10 HESS, H. F. Evaporative cooling of magnetically trapped and compressed spin-polarized hydrogen. *Physical Review B*, v. 34, n. 5, p. 3476–3479, 1986.

11 MASUHARA, N. et al. Evaporative cooling of spin-polarized atomic hydrogen. *Physical Review Letters*, v. 61, n. 8, p. 935–938, 1988.

12 SILVERA, I. F.; WALRAVEN, J. T. M. Stabilization of atomic hydrogen at low temperature. *Physical Review Letters*, v. 44, n. 3, p. 164–168, 1980.

13 SILVERA, I. F.; WALRAVEN, J. Chapter 3: spin-polarized atomic hydrogen. Available from: <https://galileo.seas.harvard.edu/images/material/334/103/Silvera1.pdf>. Acessible at: 12 Aug.2016.

14 HÄNSCH, T.; SCHAWLOW, A. Cooling of gases by laser radiation. *Optics Communications*, v. 13, n. 1, p. 68 – 69, 1975.

15 PHILLIPS, W. D.; METCALF, H. Laser deceleration of an atomic beam. *Physical Review Letters*, v. 48, n. 9, p. 596–599, 1982.

16 MIGDALL, A. L. et al. First observation of magnetically trapped neutral atoms. *Physical Review Letters*, v. 54, n. 24, p. 2596–2599, 1985.

17 CHU, S. et al. Experimental observation of optically trapped atoms. *Physical Review Letters*, v. 57, n. 3, p. 314–317, 1986.

18 RAAB, E. L. et al. Trapping of neutral Sodium atoms with radiation pressure. *Physical Review Letters*, v. 59, n. 23, p. 2631–2634, 1987.

19 WALKER, T.; SESKO, D.; WIEMAN, C. Collective behavior of optically trapped neutral atoms. *Physical Review Letters*, v. 64, n. 4, p. 408–411, 1990.

20 MONROE, C. et al. Very cold trapped atoms in a vapor cell. *Physical Review Letters*, v. 65, n. 13, p. 1571–1574, Sep 1990.

21 PRITCHARD, D. E.; HELMERSON, K.; MARTIN, A. G. Atom Traps. In: HAROCHE, S.; GAY, J.; GRYNBERG, G. (Ed.). *Atomic physics 11*. Paris: World Scientific, 1989. p. 179.

22 ANDERSON, M. H. et al. Observation of Bose-Einstein condensation in a dilute atomic vapor. *Science*, v. 269, n. ii, p. 198–201, 1995.

23 DAVIS, K. B. et al. Bose-Einstein condensation in a gas of sodium atoms. *Physical Review Letters*, v. 75, n. 22, p. 3969–3973, 1995.

24 BRADLEY, C. C. et al. Evidence of Bose-Einstein condensation in an atomic gas with attractive interactions. *Physical Review Letters*, v. 75, n. 9, p. 1687–1690, 1995.

25 MAGALHÃES, K. M. F. *Obtenção da degenerescência quântica em Sódio aprisionado*. 2004. 102 p. Tese (Doutorado em Ciências) — Instituto de Física de São Carlos, Universidade de São Paulo, São Carlos, 2004.

26 HENN, E. A. L. *Produção experimental de excitações topológicas em um condensado de Bose-Einstein*. 2008. 126 p. Tese (Doutorado em Ciências) — Instituto de Física de São Carlos, Universidade de São Paulo, São Carlos, 2008.

27 HENN, E. A. L. et al. Observation of vortex formation in an oscillating trapped Bose-Einstein condensate. *Physical Review A*, v. 79, n. 4, p. 43618, 2009.

28 HENN, E. A. L. et al. Generation of vortices and observation of quantum turbulence in an oscillating Bose-Einstein condensate. *Journal of Low Temperature Physics*, v. 158, n. 3-4, p. 435–442, 2009.

29 SEMAN, J. A. et al. Three-vortex configurations in trapped Bose-Einstein condensates. *Physical Review A*, v. 82, n. 3, p. 33616, 2010.

30 SEMAN, J. A. et al. Route to turbulence in a trapped Bose-Einstein condensate. *Laser Physics Letters*, v. 8, n. 9, p. 691–696, 2011.

31 CARACANHAS, M. et al. Self-similar expansion of a turbulent Bose-Einstein condensate: a generalized hydrodynamic model. *Journal of Low Temperature Physics*, v. 170, n. 3-4, p. 133–142, 2013.

32 HENN, E. A. L. et al. Emergence of turbulence in an oscillating Bose-Einstein condensate. *Physical Review Letters*, v. 103, n. 4, p. 45301, 2009.

33 TSATSOS, M. C. et al. Quantum turbulence in trapped atomic Bose–Einstein condensates. *Physics Reports*, v. 622, p. 1–52, mar 2016. doi: 10.1016/j.physrep.2016.02.003.

34 CHOU, T. T.; YANG, C. N.; YU, L. H. Bose-Einstein condensation of atoms in a trap. *Physical Review A*, v. 53, n. 6, p. 4257–4259, Jun 1996.

35 KU, M. J. H. et al. Revealing the superfluid lambda transition in the universal thermodynamics of a unitary Fermi gas. *Science*, v. 335, n. 6068, p. 563–567, 2012.

36 ROMERO-ROCHÍN, V.; BAGNATO, V. S. Thermodynamics of an ideal gas of bosons harmonically trapped: equation of state and susceptibilities. *Brazilian Journal of Physics*, v. 35, n. 3A, p. 607–613, 2005.

37 ROMERO-ROCHÍN, V. Equation of state of an interacting Bose gas confined by a harmonic trap, the role of the harmonic pressure. *Physical Review Letters*, v. 94, n. 13, p. 130601, 2005.

38 HENN, E. A. L. et al. Global thermodynamic variables description for a confined cold gas undergoing Bose-Einstein condensation. *Nuclear Physics A*, v. 790, n. 1-4, p. 800–803, 2007.

39 SILVA, R. R. et al. Definition and measurement of global thermodynamic variables for laser-cooled trapped gas. *Laser Physics*, v. 16, n. 4, p. 687–692, 2006.

40 ROMERO-ROCHIN, V. et al. Observation of Bose-Einstein condensation in an atomic trap in terms of macroscopic thermodynamic parameters. *Physical Review A*, v. 85, n. 2, p. 23632, 2012.

41 SHIOZAKI, R. F. et al. Measuring the heat capacity in a Bose-Einstein condensation using global variables. *Physical Review A*, v. 90, n. 4, p. 1–5, 2014.

42 POVEDA-CUEVAS, F. J. et al. Isothermal compressibility determination across Bose-Einstein condensation. *Physical Review A*, v. 92, n. 1, p. 013638, 2015.

43 BAHRAMI, a. et al. Investigation of the momentum distribution of an excited BEC by free expansion: coupling with collective modes. *Journal of Low Temperature Physics*, v. 180, n. 1-2, p. 126–132, 2015.

44 FRITSCH, A. R. et al. Nonlinear dependence observed in quadrupolar collective excitation of a trapped BEC. *Journal of Low Temperature Physics*, v. 180, n. 1-2, p. 144–152, 2015.

45 NAKAHARA, M. et al. Simple method to create a vortex in Bose-Einstein condensate of alkali atoms. *Physica B*, v. 284, p. 17–18, 2000.

46 LEANHARDT, A. E. et al. Imprinting vortices in a Bose-Einstein condensate using topological phases. *Physical Review Letters*, v. 89, n. 19, p. 190403, 2002.

47 TAVARES, P. E. S. *Excitations in Bose-Einstein condensates: collective modes, quantum turbulence and matter wave statistics.* 2016. 134 p. Tese (Doutorado em Ciências) — Instituto de Física de São Carlos, Universidade de São Paulo, São Carlos, 2016.

48 TAVARES, P. E. S. *Consequências das excitações oscilatórias em condensados de Bose-Einstein.* 2012. 103 p. Dissertação (Mestrado em Ciências) — Instituto de Física de São Carlos, Universidade de São Paulo, São Carlos, 2012.

49 SHIOZAKI, R. F. *Quantum turbulence and thermodynamics on a trapped Bose-Einstein condensate*. 2013. 129 p. Tese (Doutorado em Ciências) — Instituto de Física de São Carlos, Universidade de São Paulo, São Carlos, 2013.

50 SALINAS, S. R. A. *Introduction to statistical physics*. New York: Springer, 2001. ISBN 0-387-95119-9.

51 GREINER, W.; NEISE, L.; STÖCKER, H. *Thermodynamics and statistical mechanics*. New York: Springer, 1997. ISBN 0-387-94299-8.

52 BAGNATO, V.; PRITCHARD, D. E.; KLEPPNER, D. Bose-Einstein condensation in an external potential. *Physical Review A*, v. 35, n. 10, p. 4354–4358, 1987.

53 DALFOVO, F. et al. Theory of Bose-Einstein condensation in trapped gases. *Reviews of Modern Physics*, v. 71, n. 3, p. 463–512, 1999.

54 PETHICK, C. J.; SMITH, H. *Bose-Einstein condensation in dilute gases.* 2nd ed. Cambridge: Cambridge University Press, 2008. 569 p. ISBN 978-0-521-84651-6.

55 GROSS, E. P. Structure of a quantized vortex in boson systems. *Il Nuovo Cimento*, v. 20, n. 3, p. 454–477, 1961.

56 PITAEVSKII, L. P. Vortex lines in an imperfect Bose gas. *Soviet Physics Journal of Experimental and Theoretical Physics*, v. 13, n. 2, p. 451–454, 1961.

57 PITAEVSKII, L. P.; STRINGARI, S. *Bose-Einstein condensation*. Oxford: Oxford University Press, 2003. 382 p. ISBN 978-0-19-850719-2.

58 ROGEL-SALAZAR, J. The Gross–Pitaevskii equation and Bose–Einstein condensates. *European Journal of Physics*, v. 34, n. 2, p. 247–257, 2013.

59 SANDOVAL-FIGUEROA, N.; ROMERO-ROCHÍN, V. Thermodynamics of trapped gases: generalized mechanical variables, equation of state, and heat capacity. *Physical Review E*, v. 78, n. 6, p. 61129, 2008.

60 ZETTILI, N. *Quantum Mechanics: Concepts and Applications*. 2. ed. United Kingdom: Wiley, 2009. ISBN 978-0-470-02678-6.

61 MYATT, C. J. et al. Multiply loaded magneto-optical trap. *Optics Letters*, v. 21, n. 4, p. 290–292, Feb 1996.

62 RAPOL, U. D.; WASAN, A.; NATARAJAN, V. Loading of a magneto-optic trap from a getter source. *Physical Review A*, v. 64, n. 2, p. 23402, 2001.

63 PRITCHARD, D. E. et al. Light traps using spontaneous forces. *Physical Review Letters*, v. 57, n. 3, p. 310–313, 1986.

64 METCALF, H. J.; STRATEN, P. *Laser cooling and trapping*. New York: Springer-Verlag Inc., 1999. 323 p. ISBN 0-387-98727-9.

65 COHEN-TANNOUDJI, C. N. Nobel lecture: manipulating atoms with photons. *Reviews of Modern Physics*, v. 70, n. 3, p. 707–719, 1998.

66 CHU, S. Nobel lecture: the manipulation of neutral particles. *Reviews of Modern Physics*, v. 70, n. 3, p. 685–706, 1998.

67 PHILLIPS, W. D. Nobel lecture: laser cooling and trapping of neutral atoms. *Reviews of Modern Physics*, v. 70, n. 3, p. 721–741, 1998.

68 PETRICH, W. et al. Behavior of atoms in a compressed magneto-optical trap. *Journal of the Optical Society of America B*, v. 11, n. 8, p. 1332–1335, 1994.

69 CHU, S. et al. Three-dimensional viscous confinement and cooling of atoms by resonance radiation pressure. *Physical Review Letters*, v. 55, p. 48–51, 1985.

70 MAJORANA, E. Atomi orientati in campo magnetico variabile. *Il Nuovo Cimento (1924-1942)*, v. 9, n. 2, p. 43–50, 1932.

71 LIN, Y. J. et al. Rapid production of 87Rb Bose-Einstein condensates in a combined magnetic and optical potential. *Physical Review A*, v. 79, n. 6, p. 63631, 2009.

72 PETRICH, W. et al. Stable, tightly confining magnetic trap for evaporative cooling of neutral atoms. *Physical Review Letters*, v. 74, n. 17, p. 3352–3355, 1995.

73 ESSLINGER, T.; BLOCH, I.; HÄNSCH, T. Bose-Einstein condensation in a quadrupole-Ioffe-configuration trap. *Physical Review A*, v. 58, n. 4, p. R2664–R2667, 1998.

74 MEWES, M. O. et al. Bose-Einstein condensation in a tightly confining dc magnetic trap. *Physical Review Letters*, v. 77, n. 3, p. 416–419, 1996.

75 BERGEMAN, T.; EREZ, G.; METCALF, H. J. Magnetostatic trapping fields for neutral atoms. *Physical Review A*, v. 35, n. 4, p. 1535–1546, 1987.

76 KETTERLE, W. et al. Invited oral presentation. *OSA Annual Meeting, Toronto, Canada*, 1993.

77 KETTERLE, W.; DRUTEN, N. J. V. Evaporative cooling of trapped atoms. Available from:< http://cua.mit.edu/8.422S13/ Reading20Material/EvaporativeCoolingof TrappedAtoms.pdf>. Accessible at: 12 Aug. 2016.

78 STECK, D. A. Rubidium 87 D Line Data, available online at http://steck.us/alkalidata (revision 2.1.5,13 January 2015). Acessible at: 05 Jan. 2017.

79 MEPPELINK, R. et al. Thermodynamics of Bose-Einstein-condensed clouds using phase-contrast imaging. *Physical Review A*, v. 81, n. 5, p. 1–12, 2010.

80 LEE, T. D.; YANG, C. N. Low-temperature behavior of a dilute Bose system of hard spheres. II. non equilibrium properties*. *Physical Review*, v. 113, n. 6, p. 1406–1413, 1959.

81 ANDREWS, M. R. et al. Observation of interference between two Bose condensates. *Science*, v. 275, n. 5300, p. 637–641, 1997.

82 ANDREWS, M. R. et al. Erratum: propagation of sound in a Bose-Einstein condensate [Physical Review Letters. 79, 553 (1997)]. *Physical Review Letters.*, v. 80, n. 13, p. 2967–2967, 1998.

83 ZAREMBA, E. Sound propagation in a cylindrical Bose-condensed gas. *Physical Review A*, v. 57, n. 1, p. 518–521, 1998.

84 KAVOULAKIS, G. M.; PETHICK, C. J. Quasi-one-dimensiona1 character of sound propagation in elongated Bose-Einstein condensed clouds. *Physical Review A*, v. 58, n. 2, p. 1563–1566, 1998.

85 LANDAU, L. D. The theory of superfuidity of helium ii. *Journal of Physics-USSR*, v. 5, p. 71–100, 1941.

86 STRINGARI, S. Collective excitations of a trapped Bose-condensed gas. *Physical Review Letters*, v. 77, n. 12, p. 2360–2363, 1996.

87 GRIFFIN, A.; NIKUNI, T.; ZAREMBA, E. *Bose-condensed gases at finite temperatures*. Cambridge: Cambridge University Press, 2009. ISBN 9780521837026.

88 SIDORENKOV, L. A. et al. Bose-einstein condensation of atoms in a trap. *Nature*, v. 498, p. 78–81, 2013.

89 CASTIN, Y.; DUM, R. Bose-Einstein condensates in time dependent traps. *Physical Review Letters*, v. 77, n. 27, p. 5315–5319, 1996.

90 GRIFFIN, A.; ZAREMBA, E. First and second sound in a uniform Bose gas. *Physical Review A*, v. 56, n. 6, p. 4839–4844, 1997.

91 MEPPELINK, R.; KOLLER, S.; STRATEN, P. van der. Sound propagation in a Bose-Einstein condensate at finite temperatures. *Physical Review A*, v. 80, n. 4, p. 043605, 2009.

92 SHIN, Y. et al. Dynamical instability of a doubly quantized vortex in a Bose-Einstein condensate. *Physical Review Letters*, v. 93, n. 16, p. 6–9, 2004.